Optical Communication Systems for Smart Dust

by Yunbin Song

Thesis submitted in partial fulfillment of
the requirements for the degree of

Master of Science
in
Department of Electrical Engineering

Committee:

Dr. Richard O. Claus, Chair
Dr. Ioannis M. Besieris, Committee Member
Dr. William B. Spillman, Committee Member

August 2002
Virginia Polytechnic Institute and State University

Keywords: Smart Dust, CCR, Free-Space Optical Communication, Fiber-Optic Communication

Optical Communication Systems for Smart Dust

Yunbin Song

(Abstract)

In this thesis, the optical communication systems for millimeter-scale sensing and communication devises known as "Smart Dust" are described and analyzed. A smart dust element is a self-contained sensing and communication system that can be combined into roughly a cubic-millimeter mote to perform integrated, massively distributed sensor networks. The suitable passive optical and fiber-optic communication systems will be selected for the further performance design and analysis based on the requirements for implementing these systems. Based on the communication link designs of the free-space passive optical and fiber-optic communication systems, the simulations for link performance will be performed.

CONTENTS

Figures

Tables

1. INTRODUCTION

The purpose of this thesis is to analyze techniques for designing communication systems for millimeter-scale sensing and communication devises known as "Smart Dust." A smart dust element is a self-contained sensing and communication system that can be combined into roughly a cubic-millimeter mote to perform integrated, massively distributed sensor networks [1].

Smart dust can consist of hundreds to thousands of dust motes, each containing the capability of sensing and monitoring environmental conditions and communicating to other devices. Figure 1.1 shows the conceptual diagram of a smart dust mote. Each mote contains one or more sensors, a power supply, analog circuitry, bi-directional communication, and a programmable microprocessor. Advances in miniaturization, integration, and energy management in digital circuit, optical communications and Micro Electro-Mechanical Systems (MEMS) led to the manufacturing of small sensors, optical communication components, and power supplies, whereas microelectronics provides increasing functionality in smaller areas, with lower energy consumption [1,2].

Actual smart dust motes are being developed by professor Kris Pister at the University of California, Berkeley, as part of a program to produce the smallest possible devices that have a viable way of communicating with each other. At present, each mote is about 5 mm long as shown in Figure 1.2. A free-space passive optical communication that will be discussed in section 4 is based on their works.

Due to advantages in discreet size, substantial functionality, connectivity and low cost, smart dust will provide new methods to sense and interact with the environment. Each dust mote can be equipped with many different sensors depending on specific purposes: temperature, light, humidity, pressure, 3 axis magnetometers, 3 axis accelerometers and other sensors. Dust motes can be mounted to the objects that one wishes to monitor, or a large collection of motes can just be deployed over the environment at random.

The motes obtain the desired information from the surrounding environment and report these via a communication network. Depending on the application, dust motes can be made to only communicate directly with a base station transceiver, or peer-to-peer communication can be performed between dust motes. The applications of smart dust are numerous for industry as well as the military. Useful applications for smart dust are listed below [3].

- Collecting data for meteorological, geophysical, or planetary research
- Tracking the movements of birds, small animals, and even insects
- Virtual keyboard (Acceleration sensing glove)
    - 2 axis accelerometer on top of the each finger on a data glove
- Smart office spaces
    - temperature, humidity, and environmental comfort sensors
- Monitoring product quality
    - temperature, humidity, pressure sensors
- Defense-related sensor networks
    - acoustic, vibration, and magnetic field sensors
- Providing interfaces for the disabled

In section 2, the functions of a smart dust component required to design a fully autonomous smart dust system are described: power supplies, sensor suites, and communication conditions. With those requirements in mind, we will realize the important design parameters to design a reliable smart dust system in following section.

In section 3, several possible communication systems will be described including free-space optical links with active and passive transmitters, fiber-optic links and RF links. The advantages and disadvantages of each system will be considered. The suitable passive optical and fiber-optic communication systems will be selected for the further performance design and analysis based on the requirements for implementing these systems.

In section 4, an optical link with a passive transmitter on the dust mote will be analyzed. Basic requisites of the optical communication will be described: line of sight, and link directionality. Several design issues will be analyzed for both uplink and downlink. The signal-to-noise ratio of a free-space optical link using a corner cube retroreflector (CCR) and a CMOS image sensor receiver will be analyzed and it will provide quantitatively the feasibility of this link design and help identify critical design parameters. In this analysis, the ambient light noise by the camera would also be considered. At the end of this section, the important design parameters and characteristics of the passive optical communication will be pointed out.

In section 5, a fiber-optic link with a passive transmitter that I have designed will be discussed and analyzed. After investigating the detailed system-level analysis, the critical components to fiber-optic communication link are analyzed. Further, some of factors governing the design of transmitter and receiver components will be examined. At the end of this section, the signal-to-noise ratio of a fiber-optic link using a corner cube retroreflector (CCR) will be derived.

Based on the previous design content, simulations for link performance of the free-space passive optical and fiber-optic communication systems will be performed in section 6. Since the system has the unique characteristics of the transmitting and receiving components, a simple communication protocol for each communication system with smart dust will be designed.

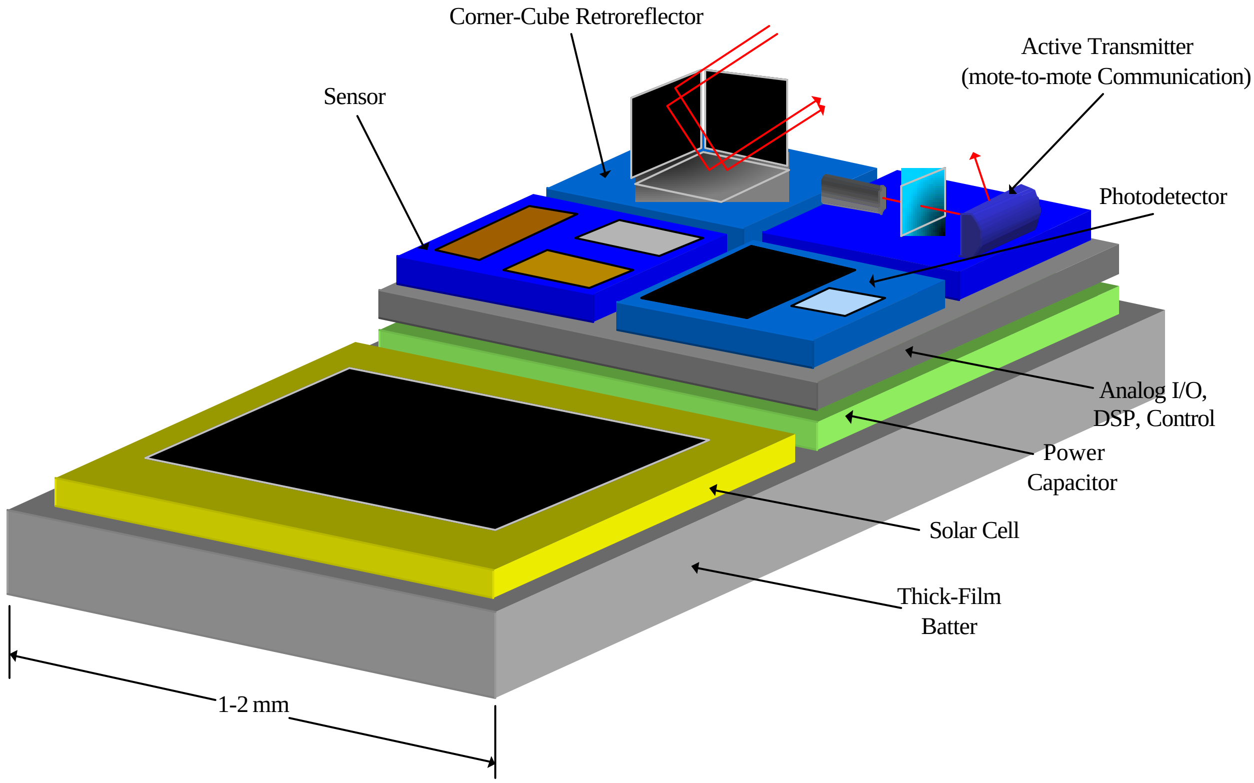

Figure 1.1: *Smart dust mote with sensor, optical receiver, passive and active optical transmitters, signal-processing and control circuitry, and power sources.*

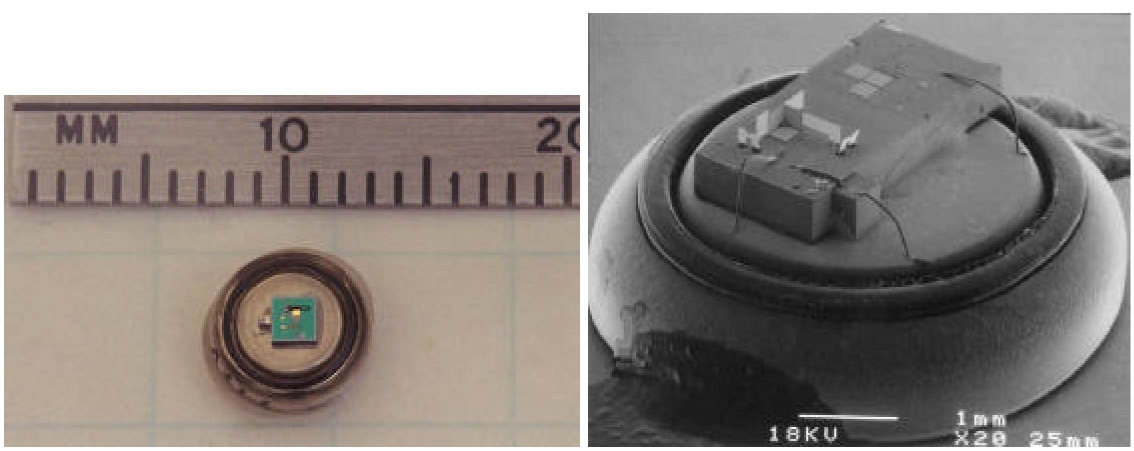

Figure 1.2: *63 mm^3 mote with a MUMPS optics chip containing a CCR for communication, a CMOS ASIC for control, and a hearing aid battery for power. [from http://www-bsac.eecs.berkeley.edu/~warneke/SmartDust/index.html]*

2. SMART DUST SYSTEM REQUIREMENTS

2.1 Power

The dust motes must have enough energy to survive anywhere from a few hours to months in order to monitor an environment. Because of the small size of the mote, energy management is a key constraint of the design. The power system consists of a thick-film battery or a solar cell with a charge-integrating capacitor to allow for charge retention for periods of darkness, or both.

Current battery and capacitor technology can store approximately 1J/mm^3 and 10mJ/mm^3, respectively, while solar cells can provide about 1J/day/mm^2 in sunlight and 1-10mJ/day/mm^2 indoors [4]. Energy consumption must therefore be minimized in every part of the system. The optical receiver of smart dust consumes approximately 0.1 nJ/bit and the transmitter uses 1 nJ/bit. The analog-to-digital converter will require 1 nJ/sample, and computations are anticipated to consume under 1pJ/instruction.

2.2 Sensor

Depending on its objective, the design integrates various sensors, including light, temperature, vibration, magnetic field, acoustic, and wind shear, onto the mote. The Micro Electro-Mechanical Systems (MEMS) industry has been growing with major markets in automotive pressure sensors and accelerometers, medical sensors, and process control sensors. Recent advances in technology have put many of these sensor processes on exponentially decreasing size/power/cost curves, and the results of this technology are of direct use here.

The sensors could be classified into two groups: weather monitors, and motion detectors. The table 1 summarizes the different types of sensors that can be used on the smart dust [5].

	Current consumption	Voltage range	Min range/ Max range	Accuracy	Temperature dependence
Magnetometer	650µA	2.7-5.25V	-/+0.5 Gauss	2 mGauss	1.4mG / °C
Accelerometer	600µA	3- 5.25V	-/+2g	25 mg	negligible
Light sensor	200µA	2.7-5.5V	0 mW/m2 /26mW/m2	6 mW/m2	negligible
Temperature Sensor	600µA	2.7-5.5V	-20°C/100°C	0.25°C	not applicable
Pressure sensor	650µA	2.7-5.5V	0.6 PSI gauge range @ 14.4 PSI absolute	2.4 mPSI	10 mPSI/°C
Humidity sensor	200µA @5V	4-9V	0-100% relative humidity	+/-2% RH	negligible

Table 1: *Sensor Specifications*

2.3 Communication

Smart dust' s full potential can only be attained when the sensor nodes communicate with one another or with a central base station. Communication system facilitates simultaneous data collection from thousands of sensors. There are several constraints in designing of the communication system due to the size and low power of dust motes. In the downlink, the central transceiver is assumed to broadcast to all of the dust motes at a bit rate of several kbps

[1]. For the uplink, each dust motes must transfer at a bit rate of 1kbps. When a smart dust ensemble employs 1,000 dust motes, an aggregate throughput is 1 Mbps.

The position of each dust mote should be identified by the central transceiver with an angular resolution of the order of 1/100 of the field of view [1]. Both uplink and downlink should be able to transfer data over a range of at least several hundred meters. The size of the dust mote transceiver should be around 1 mm^3, and each mote should require an average power not exceeding 1μW. A very low probability of data interception is preferred for both uplink and downlink. There are several secure transmission options for communicating to and from such a mote-sized cubic-millimeter computer. Radio frequency and optical communications each have their strengths and weaknesses, and are compared and contrasted in following section.

3. COMMUNICATION SYSTEM OPTIONS

In order to realize the concepts of smart dust, ultra-low-power communication should be achieved. This is one of the challenging problems in the smart dust system. The communication system is supposed to send commands to sensors on the motes and collect the reading data from the sensors. Four preliminary platforms that could be the primitive communicative functions of the smart dust will be considered: radio frequency, free-space active optical, free-space passive optical and fiber-optic communication. Each system has unique characteristics, advantages and disadvantages.

3.1 RF Communication

Radio frequency communication is one of the well-developed communication systems. It is based on the generation, propagation and detection of electromagnetic waves with a frequency range from tens of kHz to hundreds of GHz. It could be used to function as both the uplink and the downlink. Since RF transceiver typically consists of relatively complex circuitry, it is impossible to achieve the required low power operation using such an approach in a smart dust system. When large numbers of motes are involved in smart dust, RF links may employ alternative multiplexing techniques: time, frequency or code-division multiplexing. Their use leads to modulation, bandpass filtering, demodulation circuitry, and additional circuitry, all of which needs to be considered based on power consumption.

RF communication has potential for smart dust, but also poses several problems. Among the many factors included in RF communication, perhaps one of the most important problems in cubic millimeter devices is antenna size [2]. Smart mote offers very limited space for antennas. Since the size of antenna should be at least ¼ of the carrier wavelength, the limited antenna size leads to a very short wavelength [1]. In this regime, communication is not compatible with low power operation. RF communication consumes minimum power levels in the multiple milliwatt range due to analog mixers, oscillators, and filters. For example, when RF communication employs a quarter wavelength of 1 mm, the length of smart dust mote, the carrier frequency should be around 75GHz, which is not acceptable using standard RF communication methods. Nevertheless, whisker-thin antennas of centimeter length can be employed on the smart dust depending on the application. Currently, the size of a complete RF communication port is around few hundred cubic millimeters.

RF communication can be performed by using time, frequency, or code division multiplexing (TDMA, FDMA or CDMA). However, each of these techniques contains some of major factors that could not be suitable for smart dust system [1]. For example, for the case of TDMA, the dust mote should transfer at a high bit rate, as high as the aggregate uplink capacity when other multiplexing techniques are absent. Besides, dust motes should coordinate their transmission with others. In FDMA, the accurate control of oscillator frequency is required. Since CDMA operates for a relatively extended time interval, it requires high-speed digital circuitry and it consumes excessive power. Both FDMA and CDMA should avoid coordination between dust motes and they require dust motes to be preprogrammed with unique frequencies or codes in order to prevent such coordination. When smart dust employs RF communication as primary communication platform, it requires the combination of two or more of multiplexing techniques.

Space-division multiplexing (SDMA) is another multiplexing technique that we can employ in RF communication [1]. In SDMA, since the transmission from each smart dust motes should be separated from others, we need to use an antenna array in the central transceiver. Because of the limited size of the smart dust mote, SDMA would not be able to satisfy the required spatial resolution in this system. Similarly, RF communication would not be able to identify the location of the dust motes. Also, multipath propagation decreases the spatial resolution to determine the location of dust motes.

3.2 Optical Communication

Optical communication links instead employ semiconductor lasers and diode receivers to transfer and detect on/off keyed optical signals. Because of the relatively small size of the optical transceiver, optical communication may be more amenable to low-power operation than most RF communication approaches. Optical power may be collimated in tight beams even from small apertures. Diffraction effectively defines the fundamental limit on the divergence of a beam from antenna or a lens. In optical communication, the 1 GHz frequency is easily obtained from a millimeter aperture, while RF communication requires an antenna size of 100 meters across to produce collimation for a 1 GHz radio frequency signal, due to the difference in the wavelengths of the two transmissions [6]. Optical transmitters of the millimeter size can be used to obtain antenna gains of one million or more, while similarly sized radio frequency antennas are doomed by physics to be mostly isotropic.

The optical communication link has several reasons for power advantage. Optical transceivers require relatively simple baseband analog and digital circuitry. As mentioned above, the short wavelength makes a millimeter-scale device capable of emitting a narrow beam.

Also, a compact imaging receiver in the base station may be capable of decoding the simultaneous transmission from a large number of motes, at different locations.

3.2.1 Free-Space Optical Communication

Free-space optical communication, however, has two major drawbacks. First, it requires line of sight and narrow beams for accurate pointing. By using MEMS technology and clever algorithms, accurate pointing of the narrow beams can be obtained [7]. Therefore, when a line of sight path is available, smart dust can employ free-space optical links with significantly lower energy per bit than RF links. In the following sections, two approaches to optical communication will be explored: active steered laser systems and passive reflective systems.

3.2.1.1 Active Optical Communication

Active optical communication typically uses an active-steered onboard laser-diode based transmitter to send a collimated laser beam to a base station. This system contains a semiconductor laser, a collimating lens and a beam-steering micro-mirror as shown in Figure 3.1. Active optical communication is suitable for peer-to-peer communication when the application requires. Using MEMS technology, the components of the active communication network can be made to be small enough to fit into the smart dust motes [7].

One of the disadvantages of the active transmitter is its relatively high power consumption. This leads to the use of active optical communication for short duration burst-mode communication only. In order to minimize the power consumption, the active transmitter should employ some protocol to aim the beams toward the receiver: likely using directional beam and an active beam-steering mechanism. These components would make the design of the dust mote more complicated.

Active communication has the advantage of high power density. This provides capable for optical wireless communication over enormous distances. Using active optical communication, the most exciting application in peer-to-peer communication is forming multihop networks. Burst-mode communication provides the most energy-efficient way to schedule the multihop network [1]. The active laser-diode transmitter operates at up to several tens of megabits per second for a few milliseconds.

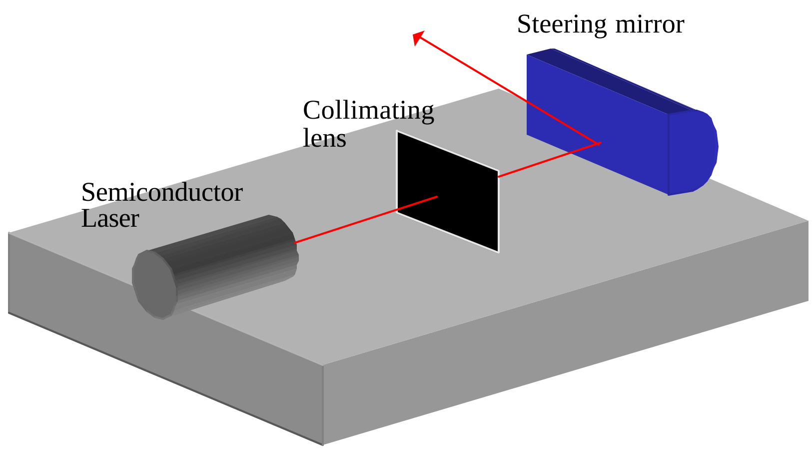

Figure 3.1: *Active transmitter on dust mote with a semiconductor laser, a collimating lens and a beam-steering micro-mirror.*

3.2.1.2 Passive Optical Communication

One of the most effective advantages in a passive optical communication system is that the dust mote does not need to have an onboard light source to transmit desired sensor information. The passive optical communication approach employs a microfabricated corner-cube retroreflector (CCR). As shown in Figure 3.2, this CCR contains three mutually perpendicular mirror fabricated of gold-coated polysilicon [8]. The CCR reflects any incident ray of light within a certain range of angles centered about the cube's diagonal back to the source. This idea comes from the fifth century B.C., when the Greeks used reflected sunlight as a beacon signal. When one of the mirrors in CCR is misaligned, the CCR would not be able to reflect signal back to the source. An electrostatic actuator in the CCR deflects one of the mirrors, and it leads to the modulation of the incident ray of light at kilohertz rates. Since the dust mote does not need to emit any light, it consumes very little power. Therefore, passive optical transmission can be performed in the smart dust system since dust motes can modulate the optical signal without having to supply any optical power.

Free space passive optical communication at visible or near infrared wavelengths (400-1600 nm) is one of the attractive communication system options for the downlink and uplink. Figure 3.3 shows a design for a bidirectional free-space optical communication link. On the downlink, the base station transceiver contains a single laser transmitter whose beam illuminates an area containing a collection of dust motes. This beam is an on-off-keyed signal containing downlink data, and commands to wake up and query the dust motes. The receiver of each dust mote consists a bandpass optical filter, a photodiode, and a preamplifier. This would involve only low-speed baseband electronics, making it far simpler that a comparable RF counterpart.

On the uplink, a special MEMS structure makes it possible for dust motes to use passive optical transmission techniques by using the corner-cube retroreflector (CCR) approach. Each dust mote can be equipped with a corner-cube retroreflector. When the illuminating beam from the base-station transmitter is not modulated, the dust mote can use this illuminating beam to transfer uplink data back to the base station by using the CCRs. The CCR reflectivity can modulate the signal at bit rates up to 10 kbps by displacing one of the mirrors in the CCR. A high frame-rate CMOS imaging system at the base-station transceiver captures these CCR signals as light blinking on and off. It decodes these blinking images to yield the uplink data.

The base station receiver contains an imaging receiver with a lens and a CCD or CMOS image sensor array. In order to synchronize the transmission from all dust motes to the frame clock of the imaging array, the imaging receiver uses periodic pulsation of the downlink or interrogating laser beam [1]. Passive optical communication using CCD has several advantages over RF communication. The short optical wavelength uses a reasonable-sized camera in the imaging receiver to obtain high spatial resolution. This enables smart dust easily to obtain information on the location of each mote, and the uplink relies upon space-division multiplexing (SDMA) [9]. The imaging receiver in the base station can obtain information via the simultaneous transmission of the 1000 dust motes without any mutual coordination.

On the other hand, passive optical communication exhibits several limitations. The communication between dust motes, so-called peer-to-peer communication, cannot be performed by passive optical communication. Since dust motes rely only on the light source of the central station to send and receive data, if a given mote does have a clear line of sight to the base station, the mote would not be able to perform any communication and this would be isolated from the system. Since each CCR can only reflect a small fraction of the illuminating light beam, the rest of illuminated light is wasted.

3.2.2 Fiber-optic communication

Fiber-optical communication employs semiconductor laser, fiber cable and diode receiver to generate, transfer and detect the optical signal. Since similar techniques to free-space passive optical communication will be employed in fiber-optic communication, most basic characteristics of the passive free-space optical communication remain the same. The relatively small size of the optical transceiver is employed with low-power operation. Each dust mote does not need to have an on board light source to transmit the data. By the using MEMS technology, Corner cube retroreflector is employed on each dust mote to modulate uplink data to base station.

Fiber-optic communication has advantages and disadvantages over a passive free-space optical communication. Since optical fiber communication employs fiber cables to transfer and receive optical signals, it does not require the unbroken line-of-sight, the link directionality, and human eye safety on an interrogating laser. Each dust mote does not need to employ more than one CCR, and the communication between dust motes and a base station can be guaranteed. In addition, it has a longer range of communication link than that of a free space passive optical communication. However, fiber-optic communication has a limitation on the application. The optical fiber cables restrict the mobility of dust mote. Since a base station should employ several optical components for fiber connection to each dust mote, it may complicate base station design.

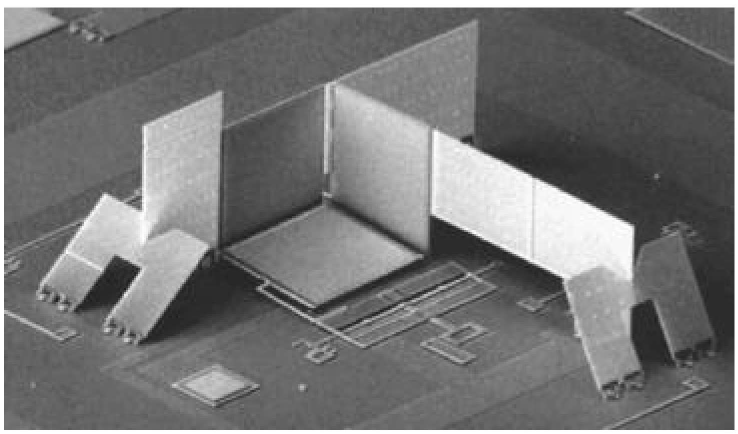

Figure 3.2: *Microfabricated corner-cube retrofrflector with three gold-coated polysilicon mirrors.*

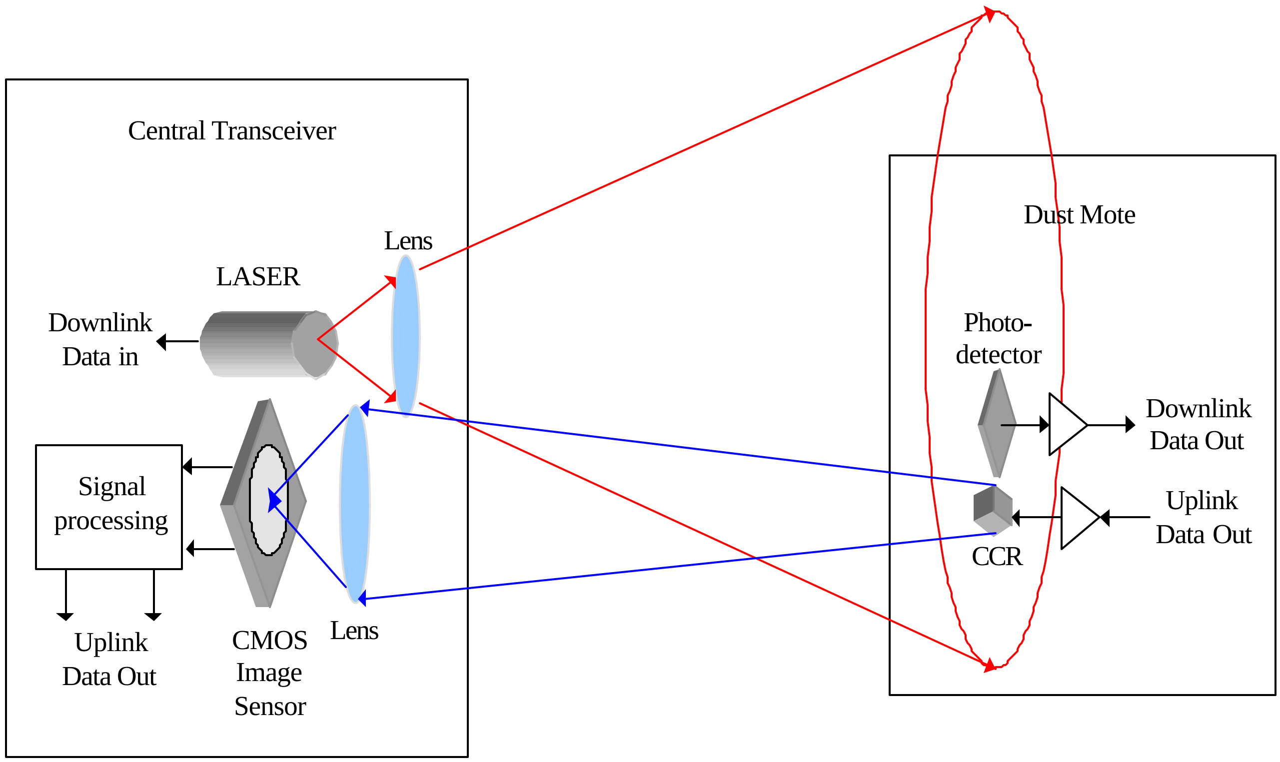

Figure 3.3: *Design of a bidirectional free-space optical communication link in which a base-station transceiver communicates simultaneously with a collection of many dust motes (only one dust mote is shown in this Figure)*

4. PASSIVE OPTICAL COMMUNICATION

The primary goal of the communication protocol for smart dust system is the data transmission ability between a central transceiver and a collection of dust motes. Based on the consideration in the previous section, the smart dust system favors free space passive optical communication for both uplink and downlink [1]. Such passive communication is very suitable for ultra-low-power communication between a central transceiver and dust motes using a low-power corner-cube-retroreflector (CCR) modulation approach.

4.1 System requirements

In order to implement passive optical communication on a smart dust system, there are some critical limitations. An unbroken line-of-sight path is required to transfer and receive optical signals. And, the directional characteristics of the CCR and optical receiver should be considered in system design.

4.1.1 Line-of-Sight Requirement

Free-space optical links for smart dust require an unbroken line-of-sight path, and rely on reflections from one or more objects between the transmitter and receiver. In order to obtain a high signal-to-noise ratio, the transmitted beam should have a small angular spread with acceptable transmitter power [1]. In most cases, specular reflection increases a beam's angular spread. A properly aligned specular reflector would not have much effect on the beam's angular spread. Diffuse reflection, however, makes the energy of the beam scatter over a wide range of angles, but usually insufficient energy toward is scattered the receiver. Diffuse, non-line-of-sight transmission is feasible only for the active transmitter, and then over a very short distance. Since diffuse, non-line-of-sight makes both the interrogating beam and the reflected beam scatter over a wide range of angles, it cannot be used to advantage in passive optical communication.

When a fixed dust mote does not have a line-of-sight path to the base station, it can communicate with the base station via a suitable multihop path. Such suitable multihop routing can be improved by higher dust mote density. However, such operation requires an active transmitter on the dust mote and increases latency. Since smart dust has a limitation on power consumption and size, low-complexity multihop routing algorithms are desired.

Depending on the application, a dust mote may be able to float in the air. In this case, an otherwise not fixed, line-of-sight path to the base station may or may not become available.

When such a path become intermittently available, the base station can continuously transfer signals to the dust mote. In such a case, the mote can also transmit a packet back to the base station. When the average time between occurrences of the availability of line-of-sight paths is longer than the packet duration, multihop routing could be used to minimize the latency.

4.1.2 Link Directionality

In most cases, the angular spread of the interrogating beam from the base station should cover the same region as the field of view of the imaging receiver in the base station [7]. This condition should be satisfied in the system using passive dust mote transmitters, and active dust mote transmitters when the system performs bi-directional transmission between the base station and dust motes. Depending on the application, using an active dust mote transmitter, the angular spread of the base station transmitter beam could be smaller than the field of view of the base station. In this case, the transmitter beam would be pointed to various locations within the field of view of the receiver.

Since a dust mote has a limitation of size, the optical receiver of the dust mote cannot employ an imaging or non-imaging optical concentrator in front of photodetector. As a result, the dust mote receiver can receive input signals from most of the hemisphere in front of the dust mote. Consequently, the transmitter beam does not have to aim at the dust mote receiver. The passive dust mote transmitter uses the CCR and the interrogating beam from the base station. The CCR reflects the interrogating beam back to the source within few tens of degrees of itscube body diagonal. When a dust mote employs only one CCR, the probability of the ability to transmit to the base station is about 10% since a dust mote should employ eight CCRs to cover all directions [7]. When a dust mote employs additional CCRs, this probability would be increased. Alternatively, MEMS aiming mechanisms can be employed with a single CCR. The accuracy of MEMS aiming mechanisms is on the order of 10 or 20 degrees. For another alternative solution, dust motes can be randomly distributed and dust motes whose CCRs happen to aim at the base station can only be considered. Dust motes can just delay transmitting until they move into an orientation that allows communication with the base station.

4.2 Link Component

As mentioned before, the passive optical communication system employs an interrogating laser, corner-cube retroreflector, and imaging senor receiver. In this subsection, the details of these major components are discussed.

4.3.1 Interrogating laser

In a passive optical communication system, the interrogating laser poses several limitations on link performance and eye safety. Interrogating lasers at the wavelengths longer than 1.4 μm are generally more suitable for human eye safety than those at shorter wavelengths [1]. However, a typical silicon photodetector at the imaging receiver is not sensitive at wavelengths beyond 1.1 μm. Since the photodetector is an important component of the optical communication system, the laser should operate at a wavelength shorter than 1.1 μm. This leads to improved eye safety by expanding the beam diameter. The diameter of the interrogating beam should be expanded until the emitted irradiance is in the eye-safe region at longer wavelengths, further in the infrared zone. Since the beam diameter of the interrogating laser is expanded, the relatively wide-aperture optical system should be also employed in the smart dust system.

In the next section, the signal-to-noise ratio (SNR) and link performance of the passive optical system will be investigated. It will be shown that the required interrogating power with a given SNR is proportional to $\lambda^{3/2}$ $[p_{bg}(\lambda)]^{1/2}$ $[\eta(\lambda)]^{-1/2}$ where p_{bg} is a spectral irradiance of ambient noise, η is the quantum efficiency of receiver and λ is a wavelength of the interrogating laser. A laser at wavelength in the visible range has many advantages. When the human eye is exposed to a high power level of optical radiation, it blinks or averts its gaze. This radiation in the visible range is better for human eye-safety than radiation in the infrared range. Furthermore, with shorter wavelength in the visible range, the factor $\lambda^{3/2}$ which is proportional to the required interrogating power can be minimized. And, the factor $[\eta(\lambda)]^{-1/2}$ can be minimized in a silicon photodetector with a thickness of a few μm. These minimizations lead to decreasing the required interrogating power of the system. Unfortunately, with current laser technology, the highest power visible laser is a 1200 mW device at a wavelength of 665 nm. Therefore, for convenience, a laser diode of 10W at a wavelength of 830nm will be used in the simulation.

4.3.2 Corner cube retroreflector

As mentioned before, the corner cube retroreflector has three mutually orthogonal planar mirrors. Any incident light within a particular solid angle is reflected back in the direction of the incident light. By moving one of the mirrors, the CCR can be used to modulate the incident ray of light at kilohertz rates. To do this, an electrostatic force is used to pull a misaligned mirror into the aligned position [10]. Then, a flexed polysilicon beam brings the mirror back to the misaligned position. Non-orthogonal alignment and curvature during the fabrication can degrade the ideal reflection efficiency. Since the reflected beam from the CCR spreads as it propagates, this leads to a fundamental limit on the performance of the long-range passive optical communication link.

As shown in Figure 4.1, a light ray along $-\hat{n}_i$ enters the CCR and changes its direction as it propagates. $\hat{n}_i$ represents the incident direction where $\hat{n}_i = n_{ix}\hat{x} + n_{iy}\hat{y} + n_{iz}\hat{z}$ with $n_{ix}^2 + n_{iy}^2 + n_{iz}^2 = 1$ [8,11]. The incident ray strikes only one of the mirrors when an incident ray is normal to one mirror. And, it strikes two of the mirrors when it is parallel to one mirror and not normal to either of the other mirrors. Any other incident ray strikes all three mirrors. The incident ray may not reflect back to the light source. This depends on both the incident direction $-\hat{n}_i$ and where the ray first makes contact. The effective active area of the mirror is the area where the incident rays that will be reflected back to the source make contact. Figure 4.2 shows how the effective area can be found in two possible cases: $2n_{iy} \geq n_{iz} \geq n_{iy} \geq n_{ix}$ and $n_{iz} \geq 2n_{iy} \geq 2n_{ix}$.

The total scattering cross section or the effective area of the CCR can be found by summing the effective areas of three mirrors [12]. The effective areas of y-z, x-z, and x-y plane are A_1, A_2, and A_3, respectively. The effective area of the entire CCR can then be expressed as following vector from.

$$s(\hat{n}_i) = \hat{n}_{ix} A_1 + \hat{n}_{iy} A_2 + \hat{n}_{iz} A_3$$

In free space optical communication, the transmission path and receive path are coincident. In order to separate the outgoing light and the incoming light, the optical communication system uses orthogonal polarizations. As shown in Figure 4.3, this can be achieved by employing a polarized beam splitter and a quarter-wave plate in the system. The interrogating light generated by the laser is linearly polarized and passes through the polarized beam splitter. After passing through a quarter-wave plate, the polarization state of the light changes to become circularly polarized. The reflected light from the CCR then propagates with the opposite circular polarization. After passing through the quarter-wave plate, it is changed to linear polarization orthogonal to the original light from the laser. Then, the polarized beam splitter will reflect it to the imaging receiver.

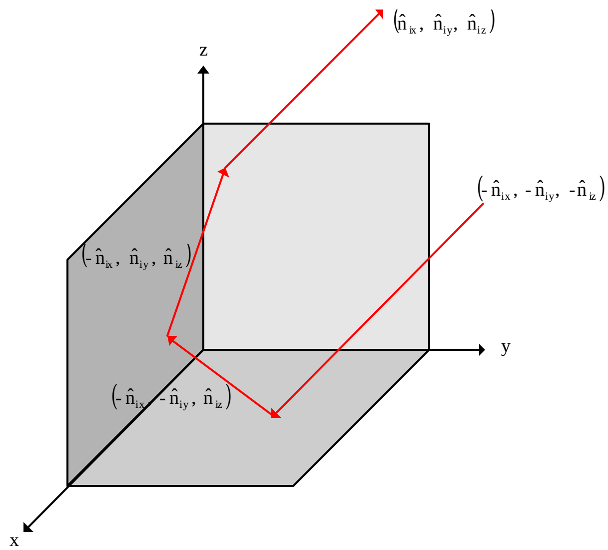

Figure 4.1: *Raytrace through CCR*

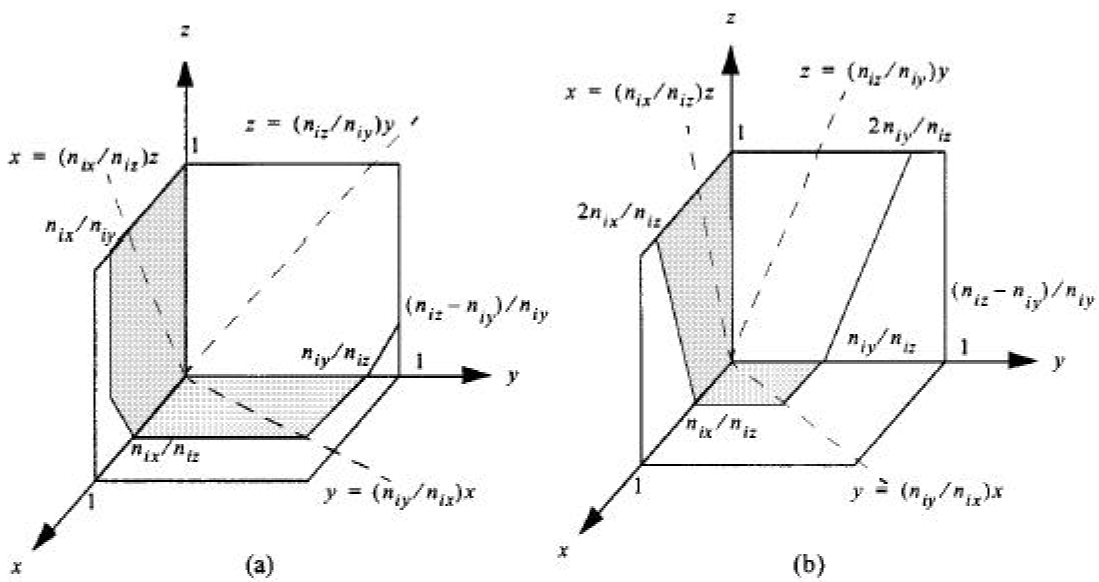

Figure 4.2: *Effective areas of CCR surfaces: (a) $2n_{iy}{}^3\ n_{iz}{}^3\ n_{iy}{}^3\ n_{ix}$ and (b) $n_{iz}{}^3\ 2n_{iy}{}^3\ 2n_{ix}$.*

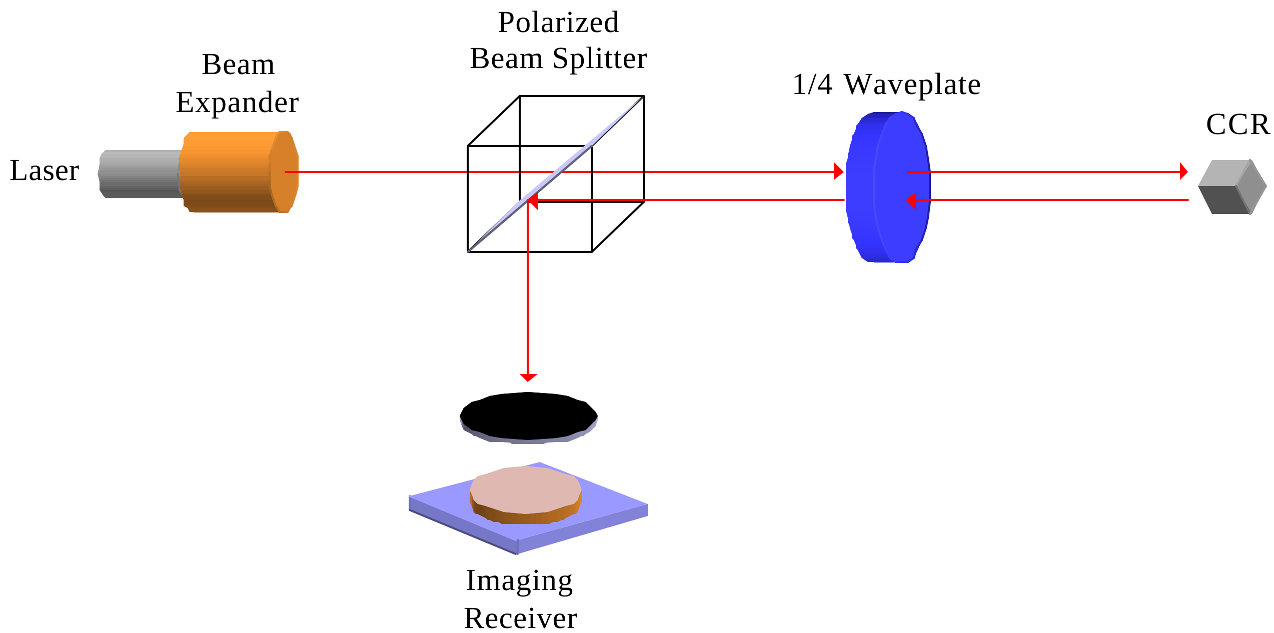

Figure 4.3: *Diagram for Separating the interrogating light and received light*

4.3.3 Imaging Receiver

A large entrance aperture of the receiver lens creates a large field of view to focus into an image. By employing a large entrance aperture, the imaging receiver can obtain more captured power from each CCR and this will improve the link SNR. The active optical image stabilization of the imaging receiver helps the imaging receiver track jittering dust mote images.

CCD and CMOS are main technologies in the imaging system. CMOS imaging systems, with active pixel sensors (APS) have many advantages over CCD imaging systems such as lower cost, increased on-chip functionality, lower power requirements, and miniaturization. Additionally, a CMOS imaging system has the ability to process incoming signals by on-chip/on-pixel processing and this will make high-data-rate reception possible [1]. Since the pulse of the interrogating laser can be synchronized with the image sensor frame clock, the frame rate should be lower than the uplink bit rate. This frame rate should also be higher than the frame rate of the most image sensor arrays.

Figure 4.4 shows the image sensor architecture. The image sensor array contains 10^5 pixels, so a representative off-chip data transfer rate can be found by multiplying a total number of pixels by the bit rate of transmission. An aggregate bit rate of the information that comes out of the image sensor array is around several tens of Mbps and this information contains the bit streams and the locations of the corresponding active pixels. As shown in Figure 4.4, the pixel array contains 1000 fixed clusters and each cluster has 100 pixels. Each cluster employs simple local circuitry that can detect active pixels, decode corresponding data, and transfer their data and location to a synchronous data bus.

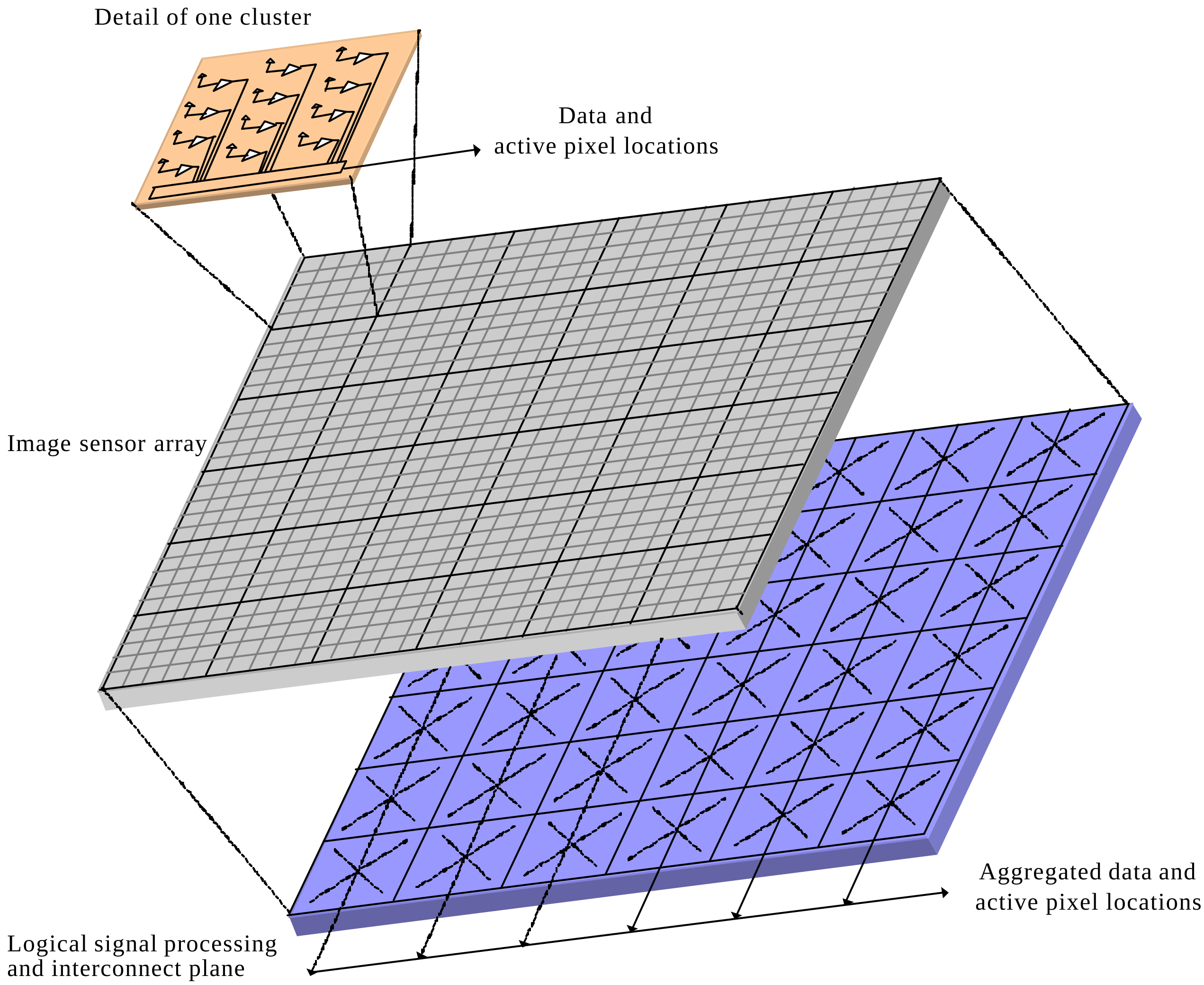

Figure 4.4: *Imaging receiver based on CMOS image sensor system.*

4.3 Analysis

In this section, a simplified mathematical approach to the analysis of the free-space passive optical communication system using CCR and CMOS image sensor receiver will be analyzed. The main object of the analysis is to determine the signal-to-noise ratio (SNR) of the communication system. Using this analysis, we may be able to estimate the overall performance of the system and critical design parameters.

4.2.1 Average received photocurrent

In this analysis, we neglect the imperfection in the CCR, atmospheric attenuation, and ambient light from the atmosphere. Let us consider the interrogating laser light that emits a CW beam at a central base station. Assume that the power of the interrogating beam is P_t and the CW beam uniformly illuminates a field of semiangle θ_f as shown Figure 4.5.

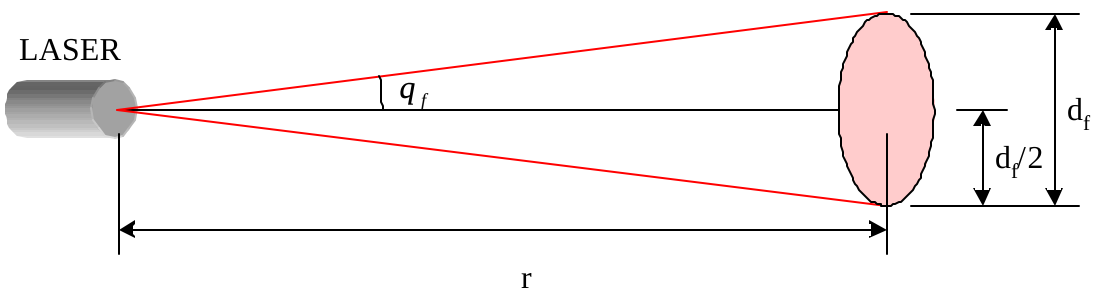

Figure 4.5: *The propagation of the interrogating laser light at a base station.*

When the distance from the interrogating laser is r, the illuminated field has a diameter d_f can be found by

$$d_f = 2r\tan\theta_f.$$

The irradiance can be defined as the radian power incident per unit area upon a surface. It is usually expressed in watts per square meter. The irradiance of the incident light I_r at a distance r from the interrogating laser can be found by

$$\text{Irradiance } (I_r) = \frac{\text{Power of CW beam}}{\text{Area}} = \frac{P_t}{\pi\left(\frac{d_f}{2}\right)^2} = \frac{P_t}{\pi r^2 \tan^2\theta_f}.$$

The interrogating light propagates to the CCR in the dust mote. The CCR has effective diameter d_c when it is not tilted with respect to the link axis. When the capture area tilted with respect to incident axis, the corresponding irradiance is proportional to the cosine of the angle θ_c between the incident axis and plane of the capture area, or the effective capture area is decreased by a factor of f_{cap}. In this case, the captured power on the CCR is

$$\begin{aligned}\text{Power}(P_{cap}) &= (\text{Irradiance}) \times (\text{effective capture area}) \\ &= (I_r)\left(\pi\left(\frac{d_C}{2}\right)^2 \cos\theta_C\right) = \frac{I_r \pi d_C^2 \cos\theta_C}{4} = \frac{P_t d_C^2 \cos\theta_C}{4r^2 \tan^2\theta_f} = \frac{P_t d_C^2 f_{cap}}{4r^2 \tan^2\theta_f},\end{aligned}$$

where θ_C is an angle between the incident axis and the plane of the CCR.

The amount of light that is returned from the surface of the CCR is characterized by the effective reflectivity R_C. Since smart dust employs a CCR on the dust mote, the retroreflected beam is returned in the same direction from which the incident beam came. The interrogating beam is modulated by one of the CCR mirrors and this generates an on-off-keyed signal with a non-return-to-zero pulse. By assuming that the probabilities of the ones and zeros are equal, the average reflected power by the CCR can be found to be

$$P_C = (P_{cap})\frac{1}{2}R_C = \frac{P_{cap}R_C}{2} = \left(\frac{P_t d_C^2 \cos\theta_C}{4r^2 \tan^2\theta_f}\right)\frac{R_C}{2} = \frac{P_t R_C d_C^2 \cos\theta_C}{8r^2 \tan^2\theta_f} = \frac{P_t R_C d_C^2 f_{cap}}{8r^2 \tan^2\theta_f}.$$

We now need to consider the diffraction of the light when the optical signal reflected by the CCR propagates back to the base station. As shown below, the diffraction effect can be modeled as a circular aperture with diameter d_c using Fraunhofer diffraction theory when the CCR is not tilted with respect to the link axis [1,13]. When the CCR is tilted, the diffracted irradiance at the base station would be reduced by a factor f_{dif}.

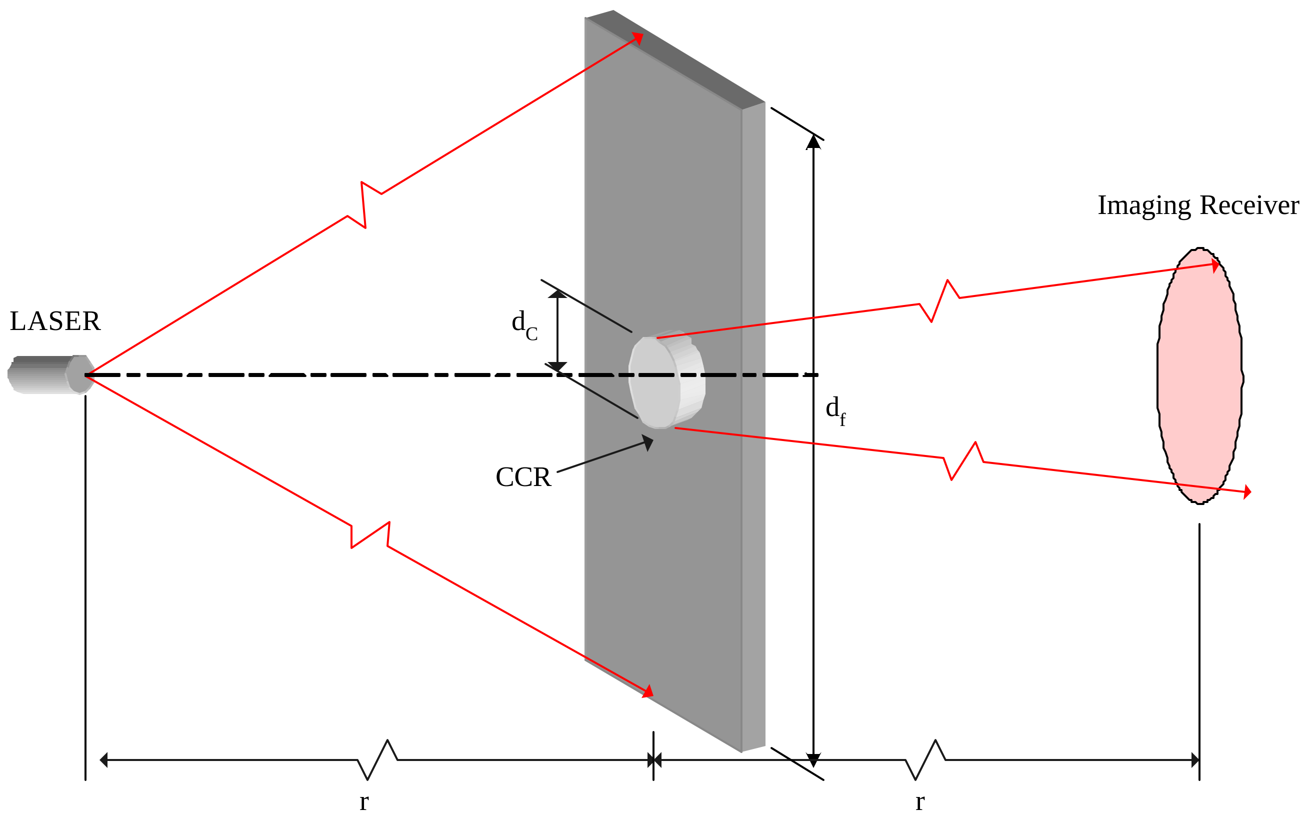

Figure 4.6: *Fraunhofer diffraction at a circular aperture.*

As investigating the Fraunhofer diffraction at a circular aperture as indicated in Figure 4.6, the intensity is given by

$$I(P) = \left[\frac{2J_1(u)}{u}\right]^2 I_0 \ ,$$

where $u = ka\sin\theta$, and $I_0 = \frac{ED}{r^2\lambda^2}$, $k = \frac{2\pi}{\lambda}$, $a = \frac{d_C}{2}$ and $D = \pi\left(\frac{d_C}{2}\right)^2$ [14,15]. The angle θ is the angle between the optical axis and the diverging wave, E is the total energy incident upon the aperture, and λ is the wavelength of the interrogating beam. Since the range of the communication link is much larger than the effective diameter of the CCR, we can treat the incident light on the CCR as a plane wave. The $\left[\frac{2J_1(u)}{u}\right]^2$ term in the above equation represents the Airy pattern of the Fraunhofer diffraction distribution for a circular aperture [16,17]. Since the diameter of CCR d_C is much smaller than the distance r between a dust mote and a base station, the intensity of the Fraunhofer diffraction can be approximated by

$$I = \frac{P_C\pi\left(\frac{d_C}{2}\right)^2}{r^2\lambda^2}.$$

Thus, when the CCR is tilted, the average irradiance at the lens of the imaging receiver can be calculated as

$$I_L = \frac{P_C\pi\left(\frac{d_C}{2}\right)^2}{r^2\lambda^2} f_{dif} = \frac{P_C\pi d_C^2}{4r^2\lambda^2} f_{dif} = \frac{\pi P_t R_C d_C^4}{32 r^4\lambda^2\tan^2\theta_f} f_{cap} f_{dif}.$$

The lens of the imaging receiver has an effective diameter d_L and a transmission T_L. Then, the output power from the lens of the imaging receiver is $I_L\, T_L\, \pi\left(\frac{d_L}{2}\right)^2$. Each pixel of the imaging receiver has a non-light-sensitive region and the fraction f_{act} expresses the sensitivity of the camera pixel to the light intensity. Thus, the output power from the camera pixel is $I_L\ T_L\ \pi\left(\frac{d_L}{2}\right)^2 f_{act}$. The imaging receiver employs an optical bandpass filter to sort the required bandwidth from the noise. This optical filter has a bandwidth $\Delta\lambda$ and a transmission T_f, and the resulting output power is $I_L\ T_L\ \pi\left(\frac{d_L}{2}\right)^2 f_{act}\ T_f$. The responsivity of the photodetector R can be defined as the ratio between the photocurrent and the incident optical power. Thus, the average received photocurrent at the imaging receiver is given by

$$i_{sig} = I_L\ T_L\ \pi\left(\frac{d_L}{2}\right)^2 f_{act}\ T_f\ R = \frac{I_L T_L \pi d_L^2 f_{act} T_f R}{4} = \frac{\pi^2 P_t d_C^4 d_L^2 T_L T_f R_C R\, f_{cap} f_{dif} f_{act}}{128 r^4 \lambda^2 \tan^2\theta_f}. \qquad (4.1)$$

4.2.2 Ambient light noise

When we analyze the performance of the communication link, we must consider the effects from the ambient noise. Ambient light comes from sunlight and other light sources. The camera at the imaging receiver receives not only the optical signal but also the ambient light noise from the CCR in the dust mote. The camera at the imaging receiver has a total of N pixels. In order to receive the optical signal from the region where the interrogating beam covers, the camera of the imaging receiver should have a field-of-view within a semiangle θ_f. The area of the CCR where each camera pixel can be viewed is $\frac{\pi\left(r \tan\theta_f\right)^2}{N}$.

Let us assume that the ambient light noise surrounding the CCR has a spectral irradiance p_{bg} and reflects the ambient light with reflectivity R_{bg}. Also assume that the optical bandpass filter at the imaging receiver has a bandwidth $\Delta\lambda$. The spectral irradiance or incident spectral radiant flux density represents the flux density in a wavelength range. The irradiance within a bandwidth $\Delta\lambda$ would be $p_{bg}\ \Delta\lambda$. Thus, the total power reflected from the area of the CCR where each camera pixel covers is given by

$$P_{bg} = \frac{\pi (r \tan\theta_f)^2}{N} \Delta\lambda \; p_{bg} \; R_{bg} = \frac{\pi \; \Delta\lambda \; p_{bg} \; R_{bg} r^2 \; \tan^2\theta_f}{N}.$$

A Lambertian reflector is a perfectly diffused reflector, which reflects electromagnetic radiation equally in all directions. This spatial distribution is typical of a classical blackbody source [13]. For such source, each part of the aperture has the same brightness as any other part. In the smart dust system, the region surrounding the CCR is effectively a Lambertian reflector [1]. So, the total power reflected from the area in the CCR diffuses out equally in all directions. Thus, the reflected irradiance at the lens within the bandwidth $\Delta\lambda$ of the bandpass filter in the optical receiver is given by

$$I_{bg} = \frac{P_{bg}}{\pi r^2} = \frac{\Delta\lambda \; p_{bg} \; R_{bg} \tan^2\theta_f}{N}.$$

As shown in the previous subsection, the transmission of the optical bandpass filter T_f, and the lens T_L, the sensitivity of the camera pixel to the light f_{act}, and the responsivity of the photodetector R must be included in the calculation for the received photocurrent from the ambient light. Thus, as done in previous section, the D.C. photocurrent per pixel due to the ambient light is given by

$$i_{bg} = I_{bg} T_L \; \pi \left(\frac{d_L}{2}\right)^2 f_{act} \; T_f \; R = \frac{I_{bg} T_L \pi d_L^2 f_{act} T_f R}{4} = \frac{\pi \Delta\lambda \; p_{bg} \; \tan^2\theta_f \, d_L^2 T_L T_f f_{act} R \; R_{bg}}{4N}. \qquad (4.2)$$

The D.C. photocurrent generates a white shot noise. The shot noise is caused by random fluctuation in the motion of charge carriers and leads to fluctuations in the current, even when the incident optical signal has constant power. The one-sided spectral density of the shot noise is given by $S = 2qi$ where q is the electron charge and i is the current [18]. Thus, the power spectral density of the shot noise per pixel can be calculated to be

$$S_{bg} = 2qi_{bg}.$$

Leakage current is the unwanted current that flows through the protective ground conductor to ground. The leakage current induces a white shot noise. Thus, the power spectral density per pixel due to the leakage current is given by

$$S_{leak} = 2qi_{leak}.$$

4.2.3 Average SNR

In this subsection, the average SNR based on the previous subsections will be derived. We need to assume that the optical signal from CCR is incident upon only one pixel, which is the best case. The imaging receiver is synchronized to the received signal. For analytical convenience, the integrator is assumed to have a gain of G.

The bit rate B is defined as the number of bits occurring per unit time in a bit stream. Each bit lasts for a certain period of time $T_B = 1/B$, known as the bit period. The imaging receiver integrates the received photocurrent for a fraction g_{int} of each bit interval. At the end of each interval, the output signal from the integrator is sampled, this sampled signal is compared to a threshold, and the binary code is used to convert each sampled value into a string of "1" and "0" bits. The average signal component of the sampled signal is $i_{sig}\, g_{int}$.

The bit rate can be expressed as $B = m f_s$ where f_s is the sampling frequency and m is the number of bits needed to code each sample. The sampling frequency can be found from the Nyquist criterion $f_s \geq 2\Delta f$, where Δf is the effective noise bandwidth. Here, the number of bits needed to code each sample can be expressed by $\frac{1}{g_{int}}$. Using the above relations, the effective noise bandwidth can be expressed in terms of the bit rate B and the fraction g_{int} of each bit interval as

$$B = m\,f_s = \frac{2\Delta f}{g_{int}} \quad \Rightarrow \quad \Delta f = \frac{B\,g_{int}}{2}.$$

The noise variance can be found by

$$s_{tot}^{2} = \left\langle i_{tot}^{2}(t) \right\rangle = \int_{-\infty}^{\infty} S_{tot}(f)\,df\ ,$$

where $i_{tot}(t)$ is the current fluctuation related to shot noise, and $S_{tot}(f)$ is the spectral density of the shot noise. Thus, the noise component of the sampled signal has a variance

$$s_{tot}^{2} = \int_{-\infty}^{\infty} S_{tot}(f)\,df = (S_{bg} + S_{leak})\,\Delta f = \frac{(S_{bg} + S_{leak})B\,g_{int}}{2}.$$

Consequently, the average SNR is given by the ratio between the average signal component and the variance of the noise component of the sample as

$$SNR_{best} = \frac{(i_{sig}\,g_{int})}{s_{tot}^{2}} = \frac{2 i_{sig}^{2}\,g_{int}}{(S_{bg} + S_{leak})B\,g_{int}}\ [1]. \tag{4.3}$$

The average probability of bit error or average bit error rate (BER) for binary modulation with a Gaussian-distributed noise source is given by

$$P_b = Q\left(\sqrt{SNR}\right),$$

where Q(x) is the Gaussian Q-function defined as

$$Q(x) = \frac{1}{\sqrt{2p}} \int_{-\infty}^{\infty} e^{-t^2/2}\,dt\ [19]. \qquad x \geq 0$$

In the imaging receiver, the received optical signal from the CCR may overlap within several pixels depending on the size of the CCR image spot, the pixel size of the image sensor, and the position of the CCR. And, the image sensor has physical gaps between pixels and non-light-sensitive region on each pixel.

There are two alternative design options to address this issue. First, in order to have a large fraction of the image spot in the light-sensitive region on the pixel, the pixel size should be comparable to the spot size. And, the shape of each pixel should be hexagonal in order to minimize the number of pixels that the CCR image spot can cover, namely N_0. When the image sensor employs the hexagonal pixels, the range of N_0 is from one to three.

For optimal performance, we can employ the maximal-ratio combining (MRC) technique to process the signals [1]. Each signal comes from the pixel that the optical signal is divided into is multiplied by the corresponding amplitude-to-noise variance ratio and from a linear combination of these signals [19,20]. For the suboptimal technique, the pixel containing the most confined signal or selecting the best of the pixels (SB) can be used. Either technique has a corresponding SNR penalty. The receiver achieves the worst SNR when the optical signal is equally divided into N_0 pixels. In this case, the SNR of MRC and SB given by

$$\mathrm{SNR}_{\mathrm{WORST}}^{MRC} = \frac{\mathrm{SNR}_{\mathrm{BEST}}}{\mathrm{N}_0}, \text{ and } \quad \mathrm{SNR}_{\mathrm{WORST}}^{SB} = \frac{\mathrm{SNR}_{\mathrm{BEST}}}{\mathrm{N}_0^2}.$$

The MRC has much better performance than the SB. Nevertheless, MRC still has a large penalty when the optical signal overlaps three or more pixels. Furthermore, to processing the MRC, we need to determine the weight of each signal that comes from the pixels and combine the signals with variable weight for the SNR estimation.

Secondly, we can just design the pixel size to be much larger than the spot size. This would make the image spot fall on only one pixel. Since the receiver does not need to employ the optimal technique, MRC or SB to perform SNR estimation, this simplifies the design of the receiver. Also, there would be no SNR penalty due to the optimal technique. If the image spot lies on the gap between pixels or non-light-sensitive region of the pixel, the receiver may not be able to receive these signals. Additionally, we can neglect these cases since we use large number of dust motes in most applications.

4.2.4 Design parameters

As we have shown in the previous subsections, there are several design parameters, which affect the performance of the passive communication link. In this subsection, these design parameter based on the derivations from the previous subsection will be analyzed. The required input interrogating power P_t depends on several design parameters. In order to find this required input power with a given SNR, we assume that the ambient induced shot noise is dominant. By combining Equations 4.1 and 4.2 into 4.3, we can express the required value of P_t as follow

$$P_t = \sqrt{\frac{4096\,\mathrm{SNR}\,r^8\,\lambda^4\,\tan^6\theta_f\;q\,B\,\Delta\lambda\;p_{bg}\,R_{bg}}{\pi^3\,d_c^8\,d_L^2\,T_L\,T_f\,R_c^2\,R\,f_{cap}\,f_{dif}^2\,f_{act}^2\,N\,\gamma_{int}}}\,.$$

As the above equation shows, the required value of P_t is proportional to r^4, $\tan^3\theta_f$, d_c^{-4}, R^{-1}, and p_{bg}.

To determine the dependence on wavelength, we need to consider the wavelength dependence of the responsivity R and the ambient light spectral irradiance p_{bg}. The responsivity of the photodetector can be expressed in terms of the wavelength as

$$R = \frac{\eta(\lambda)e}{h\nu} = \frac{\lambda\eta(\lambda)e}{hc},$$

where η is the quantum efficiency that is the ratio between the electron generation rate and the photon incidence rate, c is the speed of light in vacuum, and h is Planck's constant. When the ambient light is dominated by sunlight, the wavelength dependence of the ambient light spectral irradiance p_{bg} can be interpreted as approximating the light generated by blackbody radiation. The blackbody is defined as a theoretical object that absorbs all incident radiation. Therefore, it reflects no radiation and appears perfectly black. In practice, no material has been found to absorb all incoming radiation. Furthermore, it is a perfect emitter of radiation. At a particular temperature, the blackbody would emit the maximum amount of energy possible for the particular temperature. This value is defined as the blackbody radiation. In order to determine the blackbody radiation versus wavelength at a particular temperature, we use Planck's energy distribution formula given as

$$p_{bg}(\lambda) = \frac{2\pi\, h c^2}{\lambda^5\left(e^{hc/\lambda kT} - 1\right)},$$

where h is Planck's constant, k is the Boltzmann constant, and T is temperature. The wavelength range of interest in a smart dust system is from 400nm to 900nm and the temperature is about 300 K. With these values, the ambient light spectral irradiance $p_{bg}(\lambda)$ is approximately proportional to a factor of two. Therefore, from the above equations, the required value of P_t is proportional to $\lambda^{3/2}\ [p_{bg}(\lambda)]^{1/2}\ [\eta(\lambda)]^{-1/2}$.

5. Fiber Optic Communication

Fiber-optic communication is one of alternative communication systems for smart dust. The architecture of fiber-optic communication system is shown in Figure 5.1. For downlink, a single laser transmitter in base station generates an on-off-keyed signal containing downlink data and commands. The beam splitter divides the interrogating signals into the fibers that are connected to each dust mote. After passing through optical isolator, the interrogating signals go into directional coupler. Directional coupler divided them into two fibers. One of them will be passed while the index-matching material blocks the other. Finally, after passing lens, the interrogating signals reach to the receivers of each dust mote. On the uplink, each dust mote is equipped with a CCR. CCR modulates interrogating beams from the base station and reflects these signals back to fiber cable. The directional coupler divides the signals into two fibers. The signals in the fiber that is connected to the optical isolator will be blocked, and the signals in the other fiber will reach to the receiver in the base station.

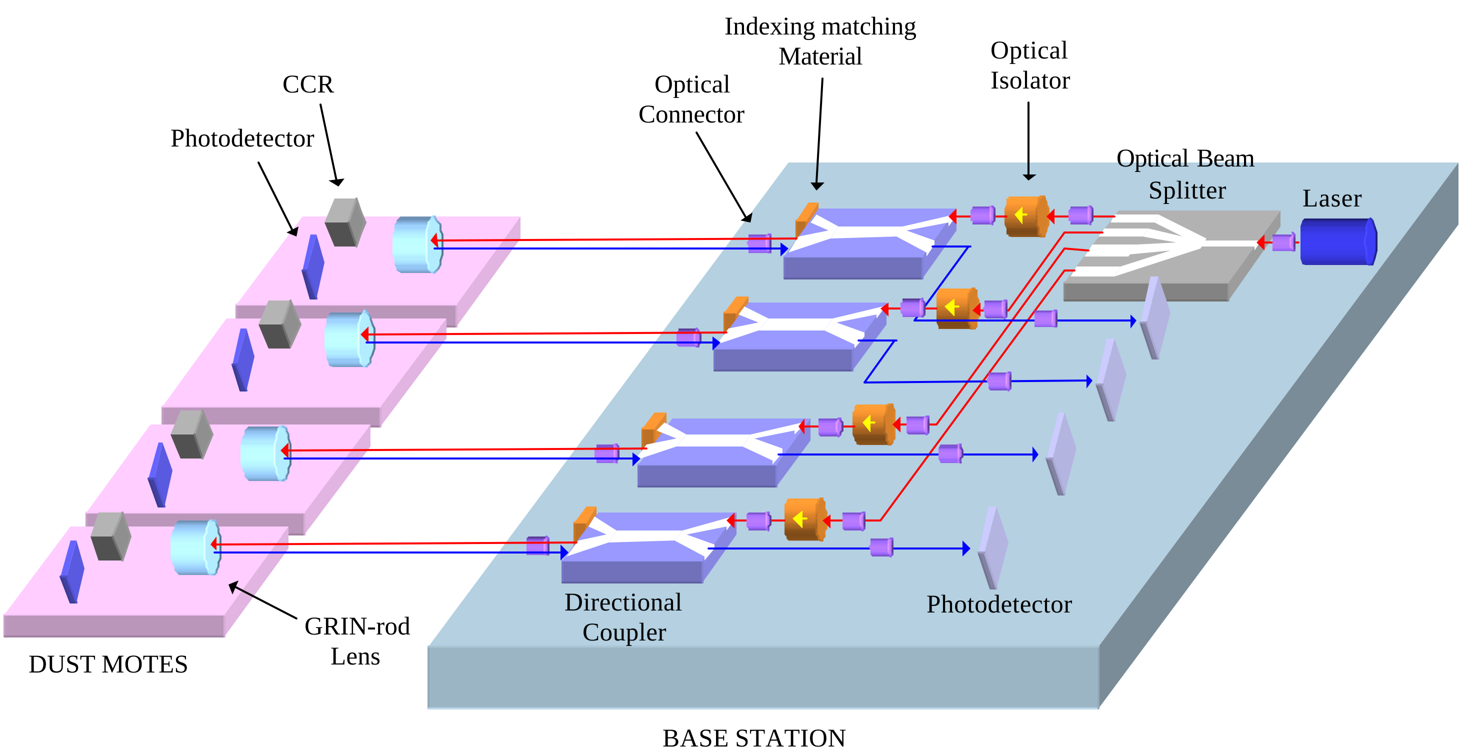

Figure 5.1: *Bidirectional fiber-optic communication link.*

5.1 Optical Fiber

An optical fiber determines the information-carrying capacity of a fiber optic communication system. The two most important characteristics of an optical fiber are pulse dispersion and loss.

5.1.1 Fiber Dispersion

Dispersion in fiber is temporal spreading of pulse. It should be obvious how this will limit bandwidth in a digital transmission system [21]. All the modes of a multimode fiber propagate with different velocities and led to the use of single-mode fibers for almost all communication application. Pulsed spread even in single-mode fibers because the spectral components of the pulse have slightly properties of the fiber. Fiber dispersion has two contributions, material dispersion and waveguide dispersion. The extent of pulse broadening for fiber of length L is found as

$$\Delta T = \mathrm{D\,L}\,\Delta l \ ,$$

where D is the dispersion parameter and is expresses in unit of ps/(km-nm) [18]. Dispersion D can be written as the sum of the material dispersion D_M and the waveguide dispersion D_W.

$$D = D_M + D_W.$$

The material dispersion and waveguide dispersion are given by

$$\begin{aligned} \mathrm{D_M} &= \frac{1}{c}\frac{dn_g}{dl} \\ \mathrm{D_W} &= -\frac{\Delta n}{c}\frac{V}{l}\frac{d^2[Vb]}{dV^2} \end{aligned}.$$

where $V = \frac{2\pi a}{\lambda}\sqrt{n_{CORE} - n_{CLAD}}$, and $b = \frac{\bar{n} - n_{CLAD}}{n_{CORE} - n_{CLAD}}$ [18]. V is a parameter, b is a normalized propagation constant, a is a core radius, n_g is a group index, $\bar{n}$ is an effective index, and n_{CORE}, and n_{CLAD} are refractive indices in core and cladding respectively. The total dispersion is zero near 1.31 μm and this wavelength refers to the zero-dispersion wavelength λ_{ZD}.

5.1.2 Fiber Loss

Fiber loss is one of the fundamental limiting factors. Since optical receiver requires a certain minimum amount of power to obtain information from the sensor motes, the transmission distance is limited by fiber loss. Fiber loss can be found as follow

$$\frac{P_{out}}{P_{in}} = 10^{-\left(\frac{\alpha L}{10}\right)} \quad \Rightarrow \quad \alpha\left(\text{dB/km}\right) = -\frac{10}{L}\log_{10}\left(\frac{P_{out}}{P_{in}}\right), \tag{5.1}$$

where L is the length of fiber, and P_{out} and P_{in} are the output power and input power respectively.

5.1.2.1 Absorptive Losses

Absorptive losses can be divided into intrinsic and extrinsic losses. Intrinsic absorption occurs when the propagating lightwave interacts with components of fiberglass's material component [21]. In the wavelength of interest to optical communication (0.8-0.9 μm and 1.2-1.5μm), intrinsic absorption can be neglected.

Extrinsic absorption is caused by the presence of minute quantities of metal ion and OH^- ions in glass. Using the vapor-phase axial deposition technique, a wide low-loss window in the silica based ultrapure fiber can be achieved.

5.1.2.2 Radiative Losses

Radiative losses are caused by the coupling of a guided light beam to radiation propagating in cladding. Rayleigh scattering is a main factor for such coupling. The attenuation coefficient due to the Rayleigh scattering in fused silica can be approximated as follow

$$a_R(l) = a_0\left(\frac{l_0}{l}\right) \text{ where } \alpha_0 = 1.7 \text{ dB/km at } \lambda_0=0.85\mu\text{m}$$

5.1.2.3 Bending Losses

Bending losses can be divided into macro and micro bending losses. For macro bending loss, a guided ray can escape out of fiber due to the bending of the fiber cable. A part of mode energy is scattered into the cladding layer. Macro bending loss is proportional to $\exp\left(\frac{-R}{R_C}\right)$, where R is radius of curvature of the fiber bend and $R_C = \frac{a}{\left(n_{CORE}^2 - n_{CLAD}^2\right)}$ [18]. For single mode fiber, R_C =0.2-0.4 µm, and the macro bending loss is less than 0.01 dB/km for R > 5mm. Since most microscopic bends are bigger than R = 5mm, macro bending losses are negligible.

Micro bending loss in fiber is caused by the random axial distortions that occur during cabling when the fiber is pressed against a surface that is not perfectly smooth causes. For single-mode fiber, micro-bending losses can be minimized by setting the V parameter to be closed to the cutoff value of 2.405 so that mode energy is confined to the core.

5.2 Link Components

Link components for optical fiber communication consist of the beam splitter, directional coupler, and optical isolator. In this section, the characteristics of these components will be discussed.

5.2.1 Directional Coupler

The optical fiber directional coupler is one of the most important fiber components. Figure 5.2.shows the architecture of the directional coupler. When two fiber cores are closed to each other, the modes of these two fibers become coupled and the input power divided into two fibers [22]. The coupling between two guides can be described by coupled wave theory as

$$\frac{P_1(z)}{P_1(0)} = 1 - \frac{k^2}{g^2}\sin^2 gz, \quad \text{and} \quad \frac{P_2(z)}{P_1(0)} = \frac{k^2}{g^2}\sin^2 gz, \tag{5.2}$$

where $g^2 = k^2 + \frac{1}{4}(\Delta b)$ and $\Delta b = b_1 - b_2$ [23]. κ is the coupling coefficient and can be measured by the strength of interaction between the two fibers. β_1 and β_2 represent the propagation constants of the modes of waveguides in two fibers. If $\beta_1 = \beta_2$, the power exchange between the two fibers is complete. On the other hand, If $\beta_1 \neq \beta_2$, the exchange of power is incomplete. When a directional coupler employs two identical fibers, the 3-dB power splitter can be achieved. Since $\beta_1 = \beta_2$, $\kappa = \beta$, and Equation 5.2 can be expressed as

$$P_1(L) = P_1(0)\left(1 - \sin^2 kL\right), \quad \text{and} \quad P_2(L) = P_1(0)\left(\sin^2 kL\right),$$

where L is a length of interaction. By setting $L = \pi/4\kappa$, two output power P_1, and P_2 can be found as

$$P_1 = \frac{1}{2} P_1(0), \quad \text{and} \quad P_2 = \frac{1}{2} P_1(0).$$

Therefore, a directional coupler acts as a 3-dB power splitter.

In a directional coupler, several characteristics can be defined as fellow [24].

$$\text{Coupling ratio (dB)} = 10 \log \frac{P_1 + P_2}{P_2}$$

$$\text{Excess loss (dB)} = 10 \log \frac{P_1(0)}{P_1 + P_2}$$

$$\text{Insertion loss (dB)} = 10 \log \frac{P_1(0)}{P_2} = \text{Coupling ratio + excess loss}$$

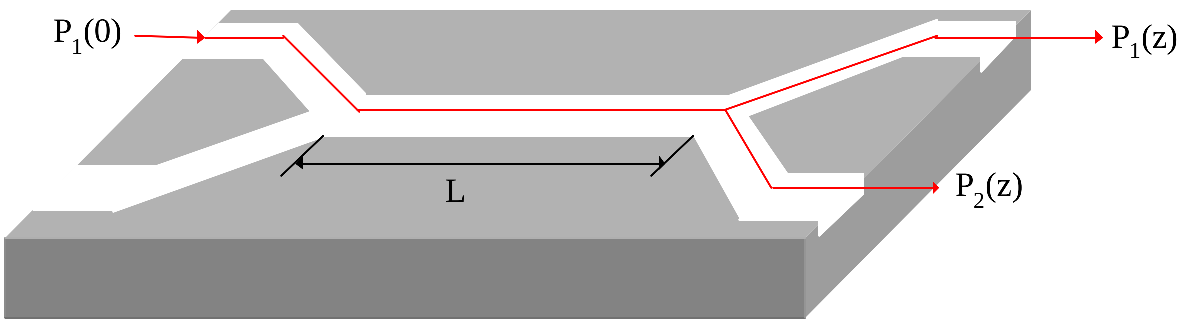

Figure 5.2: *Architecture of the directional coupler*

5.2.2 Beam Splitter

The optical bema splitter is a basic element of the optical fiber communication systems. It usually consists of the Y-junction branches. The Y-branch is a waveguide-type device and divides the received power into two channels. By combining Y-branches, the 1×N beam splitter can be achieved. A basic structure is shown in Figure 5.2 (a). Y–branch behaves as a power divider according to the branching angle and the refractive-index difference [25]. As increasing half angle θ, the power transmission of the Y-junction is decreased and the power would radiate into the substrate. Hence, the total power transmission critically depends on the angle θ. The junction should be much bigger than the width of the guide in order to achieve effective separation of the output arms.

The loss of Y-branch is mainly comes from the radiation loss at the branching point. The phase fronts of the incident waves before branching point are perpendicular to the propagation direction of the incident waveguide. Then, the incident waves propagate into two arms and they are oblique to the waveguide in the two arms. This phenomenon causes the radiation loss.

One way to decrease the radiation loss is to employ the structure shown in Figure 5.2 (b) called antenna-coupled Y-branch [26]. Since the refractive index in the n_3 region smaller than n_1 and n_2, the incident filed spreads into the n_3 region. This filed spreading makes the phase fronts of the waves to be perpendicular to the waveguide in two arms. Hence, a relatively small radiation loss can be achieved.

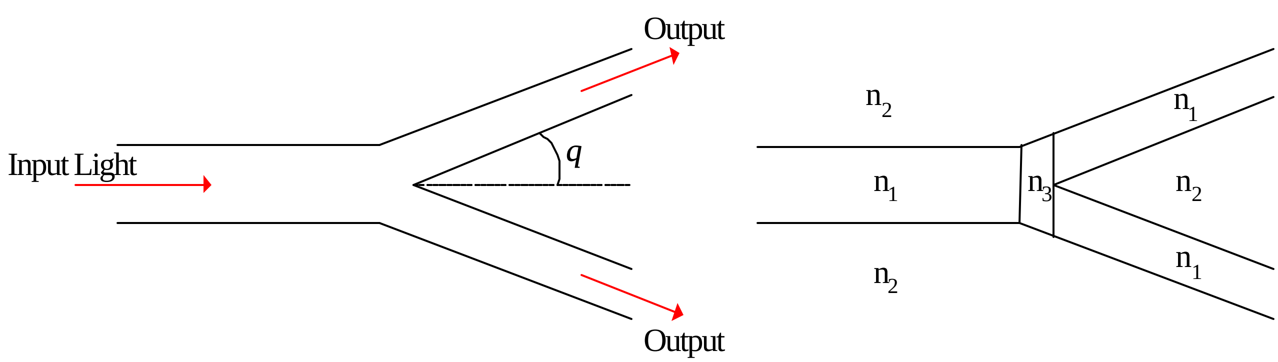

***Figure 5.3**: Y-junction beam splitter: (a) Y-branch (b) antenna-coupled Y-branch*

5.2.3 Optical Isolator

Return beams are known to have a degrading effect on the performance of fiber optic communication. To prevent such effect, optical isolators are usually employed in fiber optic communication system. Optical isolator allows the transmission of forward light but blocks the reflection of light in the reverse direction and prevents one system from disturbing another while transmitting signals between them [23]. A fiber isolator minimizes back-scattering and back-reflection of optical signals, thus maintaining a high signal-to-noise ratio.

The architecture of an optical isolator is shown in Figure 5.4. A polarizer makes the incident light to be linearly polarized. A polarization rotator rotates the polarization angle of the linearly polarized light by $\pi/4$. Then, the light comes out of the rotator would pass through an analyzer. For reflected light, an analyzer makes the polarization angle of the reflected light to be $\pi/4$, and the rotator with $\pi/4$ makes it to be $\pi/2$. A polarizer blocks the light with polarization angle $\pi/2$. The insertion loss L and isolation I can be found as

$$L = 10\log\frac{P_i}{P_t}\ , \quad \text{and} \quad I = 10\log\frac{P_i}{P_t}.$$

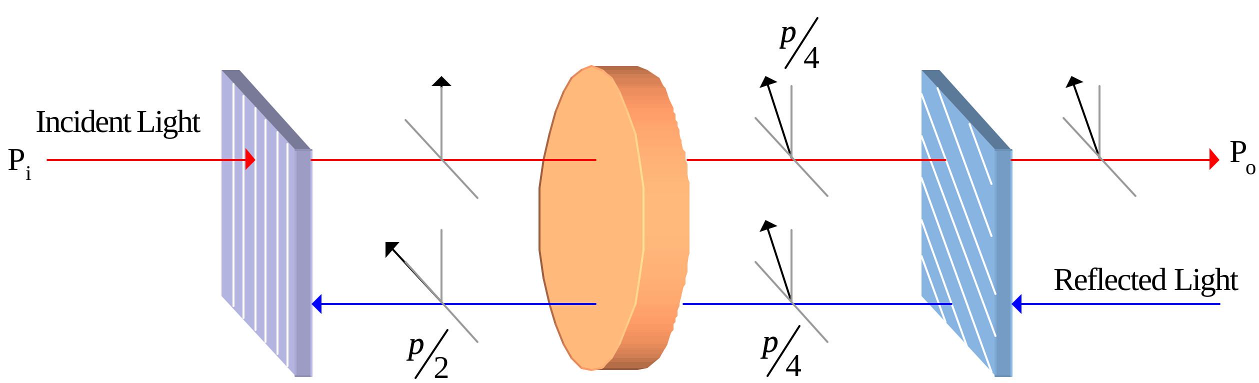

Figure 5.4: *Structure of optical isolators*

5.2.4 Index-matching material

Index-matching material is a substance, which has an index of refraction that is pretty closed to an index of refraction of an optical fiber. It is used to reduce Fresnel reflection at the fiber endface. In optical fiber communication for smart dust, the index-matching materials are employed at the end of directional coupler to avoid reflection from the fiber endface.

5.2.5 GRIN-rod Lens

The graded index (GRIN)-rod lens is a cylindrical glass rod that contains a parabolic graded refractive index profile with a maximum at the centre [23]. This property of the lens leads to developments on graded index fiber waveguide. GRIN-rod lens can be used to expend and collimate an incoming light beam or focus an incoming light to a small area located at the center of opposite lens face. Light propagation through the lens can be determined by the lens dimension and wavelength of incident light.

By using the paraxial ray equation, the ray propagation through GRIN-rod lens can be approximately described as

$$\frac{d^2 r}{dz^2} = \frac{1}{n}\frac{dn}{dr}, \tag{5.3}$$

where r is a radial coordinate, z is the optical axis coordinate and n is the refractive index of the medium. The refractive index in a graded-index medium can be expressed by

$$n(r) = n_1\left(1 - \frac{Ar^2}{2}\right), \tag{5.4}$$

where A is a positive constant and n_1 is a refractive index on the optical axis. By substituting Equation 5.3 in Equation 5.4, the ray propagation is expressed as:

$$\frac{d^2 r}{dz^2} = -Ar \,. \tag{5.5}$$

The general solution of Equation 5.5 can be found as:

$$r = K_1 \cos\left(\sqrt{A}\,z\right) + K_2 \sin\left(\sqrt{A}\,z\right),$$

where K_1 and K_2 are constants. Therefore, all the incoming rays propagate a sinusoidal path through the GRIN-rod lens. The lens can be modified by changing the period (pitch) of the sinusoidal path.

The 0.25 pitch GRIN-rod lenses are used in each dust mote as shown in Figure 5.5. The 0.25 pitch lens produces a perfectly collimated output beam when the incoming beam from a fiber. And, it focuses a reflected beam from a CCR back to the fiber. Since the focal point of the 0.25 pitch GRIN-rod lens is coincident with the lens face, it provides an efficient direct butt connection to optical fiber.

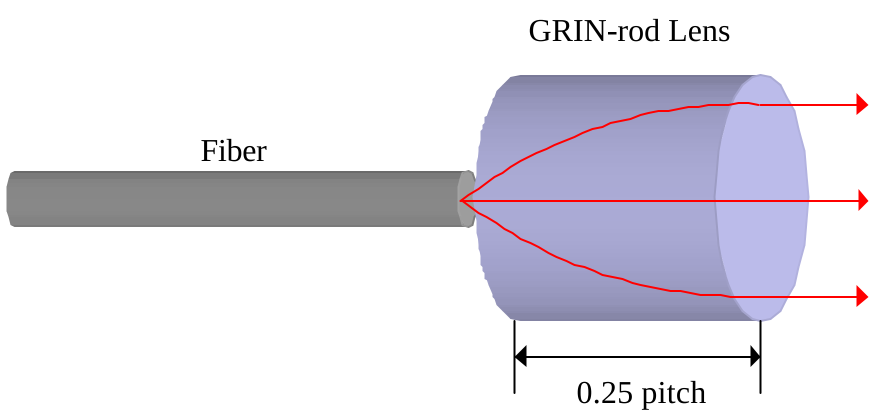

Figure 5.5: *Formation of a expanded and collimated output of beam from 0.25 pitch GRIN-rod lens*

5.2.6 Fiber connector

Fiber connector is one of the important components of fiber-optic communication system. The connector is a mechanical device connected to the end of a fiber cable. This device is designed to connect a fiber with another optical device [25]. In following subsection, various types of the fiber connectors will be discussed [23,27].

- **Traded connector**

  The threaded type of connector is used by a sub-multi assembly (SMA) connector. This connector is a first generation connector. One problem associated with this connector is the air-gap in a poor connection. This poor connection generates a change in the index of refraction and it leads to a Fresnel reflection loss in fiber optic communication system.

- **Bayonet connector**

  Bayonet connector is a more advanced type of connector than the threaded connector. This device employs a twist-turn fastening operation that reduces the possibility of the generating an air-gap. Two popular bayonet connectors are the straight tip (ST) and ST-II connectors pioneered by AT&T.

- **Push-pull connector**

  Push-pull connector uses a ceramic ferrule. The ferrule is functioned as an alignment mechanism in this fiber connector. One popular push-pull connector is the stick and click (SC) connector including a locking tab. This connector is used primarily with single-mode fiber cable.

5.3 Analysis

In this section, a simplified mathematical approach to the fiber-optic communication will be achieved. Based on the power budget of the link, the signal-to-noise ratio (SNR) of the communication system can be determined. Using this analysis, the performance of the link and critical design parameter can be estimated.

5.3.1 Downlink

Based on the simplified diagram of the fiber-optic link design in Figure 5.6, a simple power budget of the link components can be achieved. A single laser transmitter in base station generates an on-off-keyed signal with optical power P_L at wavelength λ of 1310 nm. Using the power budget of the link components, the output power of the base station P_{BSout} can be found by

$$P_{BSout} = P_L \times 10^{-\frac{Insertionloss[dB]}{10}}.$$

Since the optical fiber has a zero dispersion wavelength at 1312 nm, dispersion in single mode fiber can be neglected. The optical fiber has an attenuation coefficient α and it is expressed in units of dB/km. By using Equation5.1, the output power of the optical fiber P_{GRID} can be found as

$$P_{GRIN} = P_{BSout} \times 10^{-\frac{a}{10}L},$$

where L is a length of the optical fiber in units of km.

The 0.25-pitch GRID-rod lens has a diameter of the collimated output beam d_G. Hence, the irradiance incident upon the CCR I_C is

$$I_C = \frac{P_{GRIN}}{p\left(\frac{d_G}{2}\right)^2} = \frac{4P_{GRIN}}{p\ d_G^2}.$$

As done in section 4.2.1, the captured power on the CCR P_{cap} is

$$P_{cap} = I_C\, p\left(\frac{d_C}{2}\right)^2 f_{cap},$$

and the average reflected power by the CCR P_C can be found

$$P_C = \frac{P_{cap} R}{2}.$$

5.3.2 Uplink

After reflecting by the CCR, the signal propagates into the optical fiber again. As done in previous subsection, the average output power of the fiber P_{Bsin} is

$$P_{BSin} = P_C \times 10^{-\frac{a}{10}L},$$

and the input average optical power to the photodetector P_{PIN} can be found by

$$P_{PIN} = P_{BSin} \times 10^{-\frac{Insertionbss[dB]}{10}}.$$

The photodetector has a responsivity R, a dark current I_d at 300K, a load resistance R_L and a bandwidth $\Delta\lambda$. Thus, the average photocurrent of the receiver is

$$I_S = P_{PIN} \times R \, . \tag{5.6}$$

The shot noise power of the receiver can be found by

$$I_{SN}^2 = 2\, q\, \Delta l\, \left(I_S + I_d\right), \tag{5.7}$$

where q is an electrical charge. The thermal noise power can be also found by

$$I_{TH}^2 = \frac{4\, K\, T\, \Delta l}{R_L}, \tag{5.8}$$

where T is a temperature and K is the Boltzmann's constant. Finally, The signal-to-noise ratio can be found as

$$\mathrm{SNR} = \frac{I_S^2}{I_{SN}^2 + I_{TH}^2}. \tag{5.9}$$

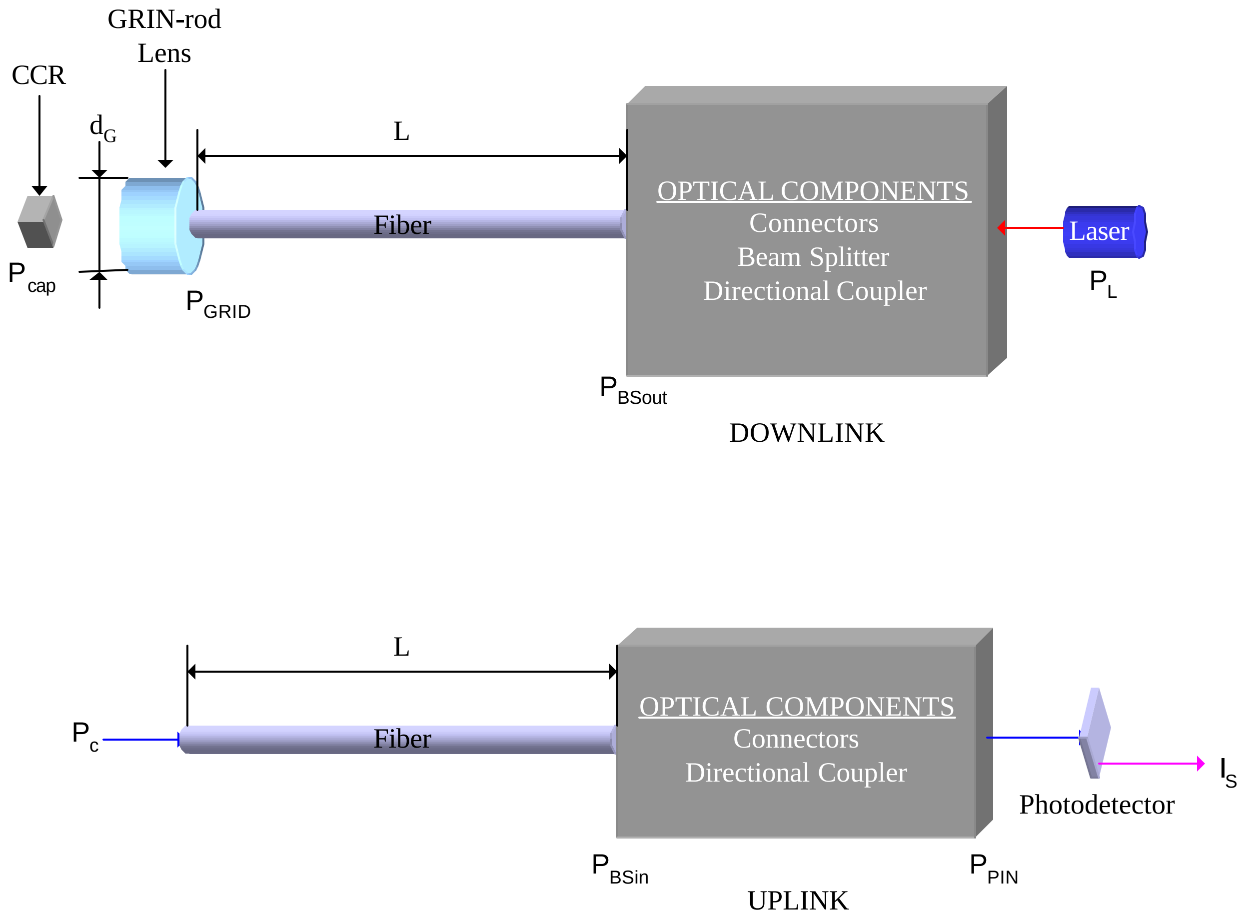

Figure 5.6: *A simplified diagram of the fiber-optic link design*

6. NETWORK PERFORMANCE

In this section, the performances of the free-space passive optical communication system and fiber-optic communication will be investigated. The typical values of design parameters are used to analyze the performance of the links based on the previous link analysis [1]. The signal-to-noise ratio (SNR), a minimum detectable power (MDP) and a maximum rage of link will be derived based on the practical design parameters.

6.1 Free-space passive optical communication

Table 2 lists the typical values of design parameters for the free-space optical communication. Based on these design parameters, the performance of the free-space passive optical communication can be achieved by link analysis from Chapter 4.

The distance of the propagating signal versus corresponding signal-to-noise ratio and average received photocurrent are shown in Figure 6.1 (a) and (b) when an interrogating power is 10 W. As shown in Equation 4.1, an average received signal is proportional to $1/r^4$. Hence, the average received signal is rapidly decreased as the signal propagates. The distance of the propagating signal versus corresponding signal-to-noise ratio with various input power are shown in Figure 6.2.

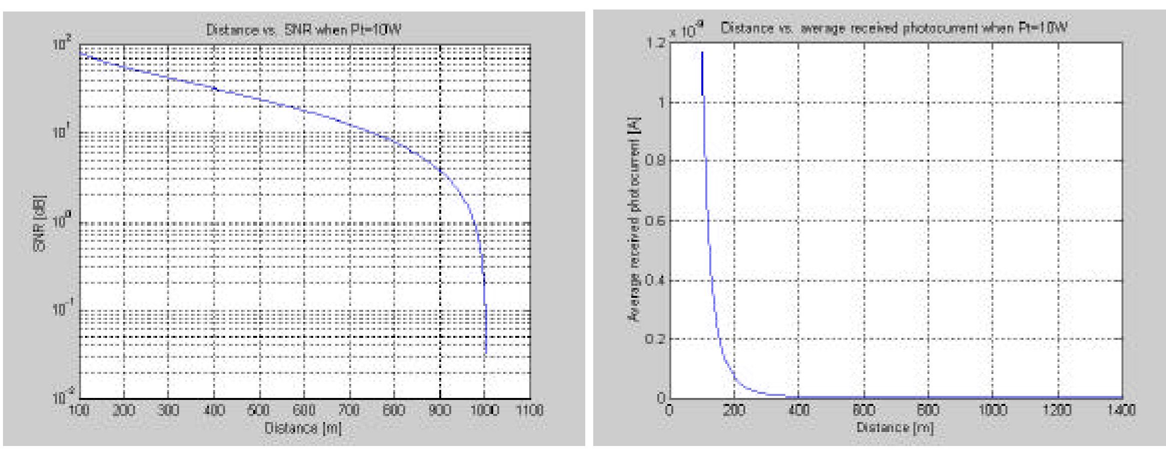

Figure 6.1: *For the free-space passive optical communication, the distance of the propagating signal versus corresponding signal-to-noise ratio and average received photocurrent when an interrogating power is 10 W: (a) distance versus SNR and (b) distance versus average received photocurrent.*

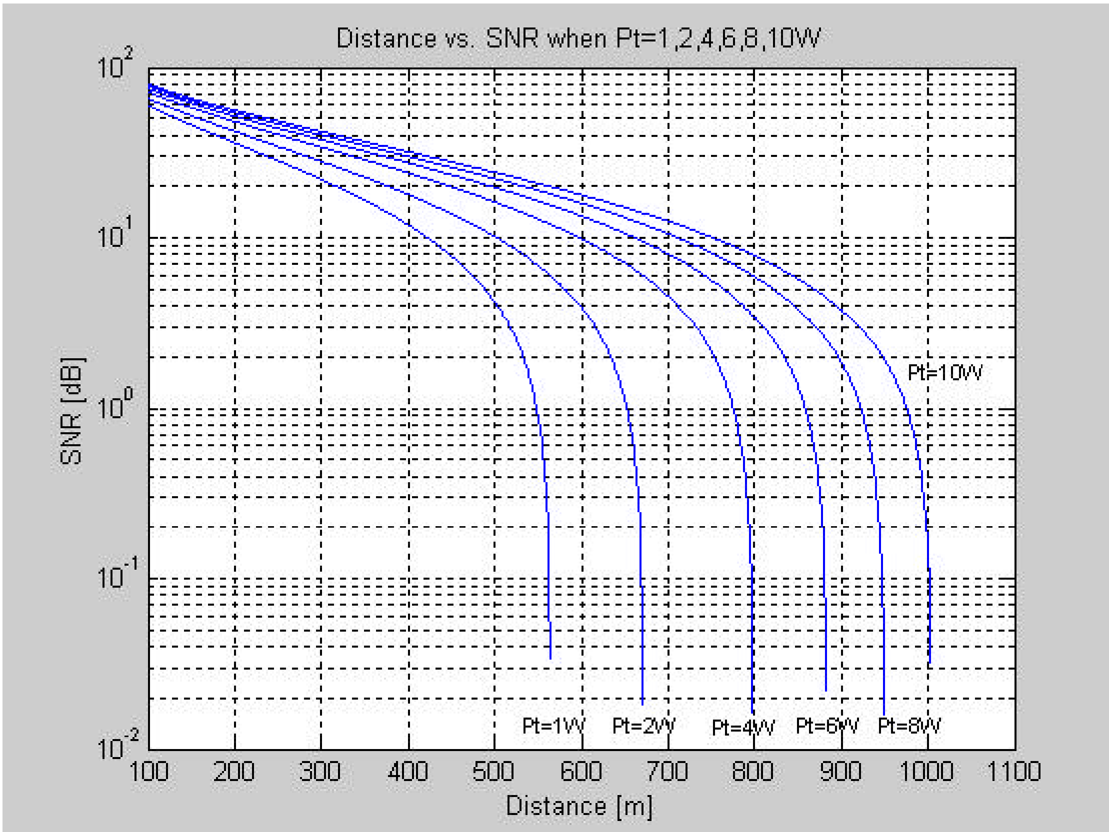

Figure 6.2: *For the free-space passive optical communication, the distance of the propagating signal versus corresponding signal-to-noise ratios with various interrogating powers.*

For the image receiver at the base station, minimum detectable power is defined as the average received power that yields unity SNR. The SNR for an image receiver from Equation 4.3 is given by

$$\mathrm{SNR} = 1 = \frac{(\mathrm{i}_{\mathrm{sig}}\, \mathrm{g}_{\mathrm{int}})}{s_{\mathrm{tot}}^{2}} = \frac{2\mathrm{i}_{\mathrm{sig}}^{2}\, \mathrm{g}_{\mathrm{int}}}{(\mathrm{S}_{bg} + \mathrm{S}_{leak})\mathrm{B}\, \mathrm{g}_{\mathrm{int}}}\,. \tag{6.1}$$

Since the responsivity of the photodetector R can be defined as

$$R = \frac{i_{sig}}{P_r}, \tag{6.2}$$

where P_r is a minimum detectable power. By substituting Equation 6.1 into Equation 6.2, the minimum detectable power can be found by

$$P_r = \frac{1}{R}\sqrt{\frac{(S_{bg} + S_{leak})B}{2\,g_{int}}} = 2.3058 \times 10^{-13}. \tag{6.3}$$

At a given wavelength, the noise-equivalent power (NEP) can be defined as the required incident power to produce a photocurrent equal to the noise current within a unit bandwidth. Hence, NEP can be obtained from Equation 6.3:

$$NEP = \frac{1}{R}\sqrt{\frac{(S_{bg} + S_{leak})}{2\,g_{int}}} = 2.3058 \times 10^{-15}.$$

From the calculation of a minimum detectable power, a maximum range of a free-space passive optical link with a particular input power can be achieved. By substituting Equation 4.1 into Equation 6.1, a maximum range of the link r_{MAX} can be found by

$$r_{MAX} = \left(\frac{g_{int}\; d_c^8\, p^4\; d_l^4\; P_t^2\; f_{cap}^2\; R_c^2\; f_{dif}^2\; T_f^2\; T_l^2\; f_{act}^2\; R^2}{8192\;\; l^4\; \tan^2 q_f\; (S_{bg} + S_{leak})} \right)^{\frac{1}{8}}.$$

The various input powers versus corresponding maximum ranges of the links are shown in Figure 5.3.

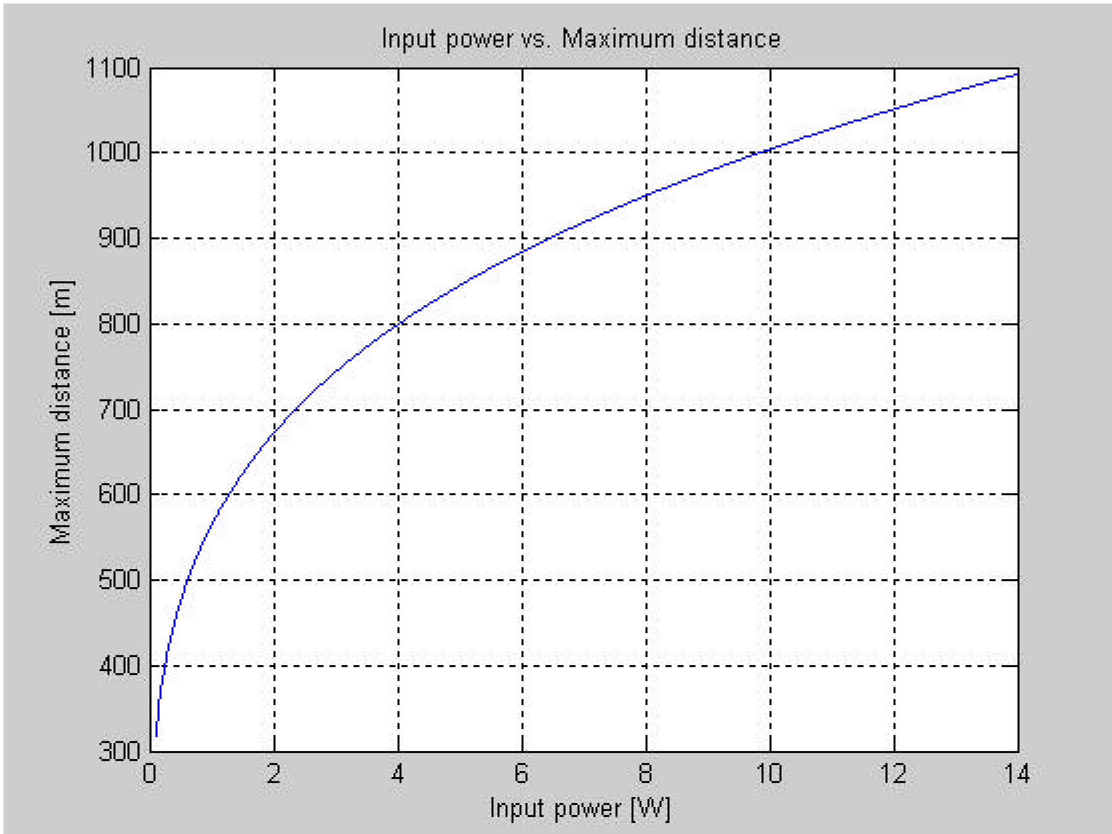

Figure 6.3: *The input powers versus corresponding maximum ranges of the free-space passive optical link.*

Symbol	Description	Typical value	Units
q_f	Semiangle of illuminated field	1	degrees
d_c	Effective diameter of CCR when not tilted	5×10^{-4}	m
R_c	Effective reflectivity of CCR	0.85	W/W
f_{cap}	Reduction of effective capture area when tiled	0.5	W/W
f_{dif}	Reduction of diffracted irradiance due to CCR tilted	0.5	W/W
λ	Interrogation wavelength	830	nm
$\Delta\lambda$	Optical bandpass filter bandwidth	5	nm

T_f	Optical filter transmission	0.8	W/W
T_l	Effective transmission of camera lens	0.8	W/W
d_l	Effective diameter of camera lens	0.1	m
R	Responsivity of photodetector	0.5	A/W
f_{act}	Fraction of camera pixel area that is sensitive to light	0.75	m^2/m^2
p_{bg}	Ambient light spectral irradiance (bright sunlight)	0.8	W/m^2-nm
R_{bg}	Reflectivity of the region surrounding CCR	0.3	W/W
N	Number of pixels in image sensor	10^5	-
i_{leak}	Leakage current per pixel	10^{-12}	A
B	Bit rate of on-off-keyed link	10^4	bps
g_{int}	Fraction of bit interval during which camera integrates	0.95	s/s

Table 2: *Typical values of design parameters for free-space optical communication*

6.2 Fiber-optic communication

In this subsection, the performance of a fiber-optic communication will be analyzed base on the practical optical fiber components with particular specifications. In this analysis, eight dust motes are employed. Table 3 lists the typical values of design parameters for the practical optical fiber components. Based on these design parameters, the performance of the fiber-optic communication can be achieved by link analysis from Chapter 5.

The distance of the propagating signal versus corresponding signal-to-noise ratio and average received photocurrent are shown in Figure 6.4 (a) and (b) when an interrogating power is 1 mW. As shown in previous chapter, an average received signal is is proportional to $10^{-2\frac{a}{10}L}$ and linearly proportional to the insertion losses of the components. Hence, the average received signal is relatively slowly decreased as the signal propagates. The distance of the propagating signal versus corresponding signal-to-noise ratio with various input power are shown in Figure 6.5.

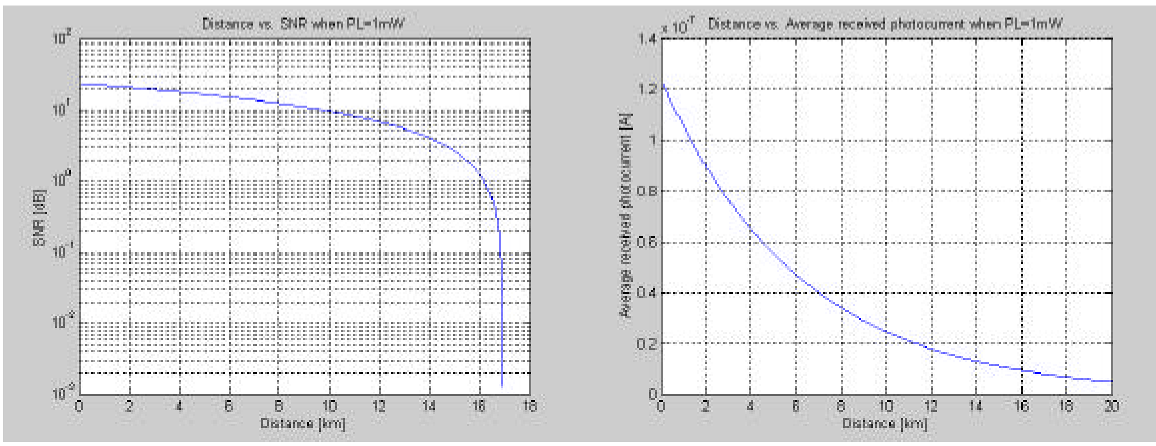

Figure 6.4: *For the fiber-optic communication, the distance of the propagating signal versus corresponding signal-to-noise ratios and average received photocurrent when an interrogating power is 1 mW: (a) distance versus SNR and (b) distance versus average received photocurrent.*

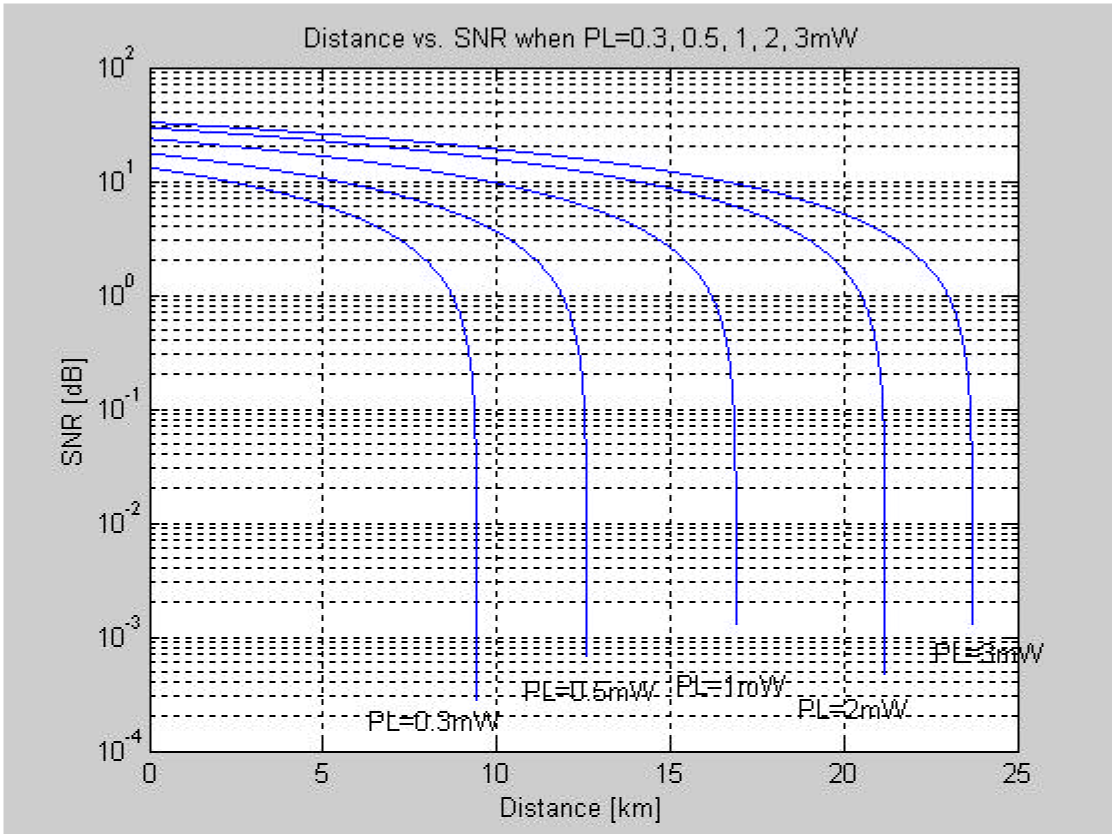

Figure 6.5: *For the fiber-optic communication, the distance of the propagating signal versus corresponding signal-to-noise ratios with various interrogating powers.*

As mentioned in previous subsection, for the photodetector at the base station, minimum detectable power is defined as the average received power that yields unity SNR. The SNR for an image receiver from Equation 5.9 is given by

$$\mathrm{SNR} = 1 = \frac{\mathrm{I}_{\mathrm{S}}^2}{\mathrm{I}_{\mathrm{SN}}^2 + \mathrm{I}_{\mathrm{TH}}^2}. \tag{6.4}$$

Since the responsivity of the photodetector R can be also defined as

$$\mathrm{R} = \frac{\mathrm{I}_{\mathrm{S}}}{P_r}, \tag{6.5}$$

where P_r is a minimum detectable power. The I_S is assumed to be much smaller than I_d. Then, by substituting Equation 6.5, 5.6, 5.7 and 5.8 into Equation 6.4, the minimum detectable power can be found by

$$P_r = \frac{1}{R}\sqrt{\Delta f\left(2\,q\;I_d + \frac{4\,K\,T}{R_L}\right)} = 9.5843\times10^{-9}\,. \tag{6.6}$$

At a given wavelength, the noise-equivalent power (NEP) can be defined as the required incident power to produce a photocurrent equal to the noise current within a unit bandwidth. Hence, NEP can be obtained from Equation 6.6:

$$NEP = \frac{1}{R}\sqrt{2\,q\;I_d + \frac{4\,K\,T}{R_L}} = 1.5154\times10^{-12}\,.$$

From the calculation of a minimum detectable power, a maximum range of a free-space fiber-optic link with a particular input power can be achieved. By using Equation 5.6, 5.7 and 5.8 and 6.4 under the previous assumption, a maximum range of the link r_{MAX} can be found by

$$L_{MAX} = \frac{\log_{10}\left[\dfrac{4\,d_G^2\,\left(2\,q\,\Delta f\;I_d + I_{TH}\right)}{P_L^2\,d_C^4\,f_{cap}^{\,2}\,R_C^2\,R^2}\right] + 4.1}{-0.14}\,.$$

The various input powers versus corresponding maximum ranges of the links are shown in Figure 5.3.

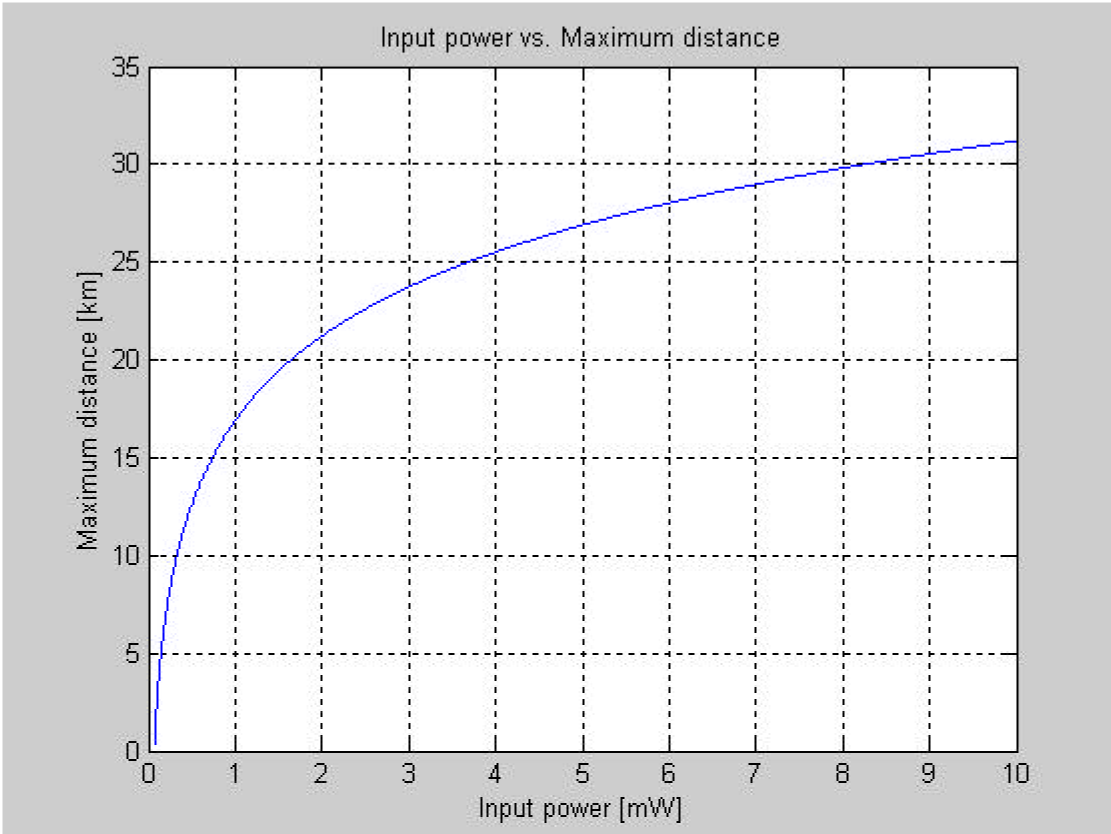

Figure 6.6: *The input powers versus corresponding maximum ranges of the fiber-optic link.*

Component	Product	Specification
Optical Fiber	CORNING PI1042	Single mode fiber Attenuation ≤ 0.35 dB/km Core diameter = 8.3 µm Zero dispersion wavelength = 1312 nm Numerical Aperture = 0.13
Laser	NOTEL LC131-98	Mean output power = 1dBm Wavelength = 1310 nm
Fiber connector	FITEL SC/PC-2-S	Insertion loss ≤ 0.3 dB
Optical beam splitter	FWGC-SM-1×8	Insertion loss ≤ 11 dB Uniformity ≤ 1.0 dB

Optical isolator	SUMITOMO SE-13S	Insertion loss ≤ 0.5 dB Isolation ≥ 40 dB
Directional coupler	DELTA OPC-KA5A4-33500	Coupling Ratio = 50/50 Insertion loss ≤ 3.6 dB
GRIN-rod lens	GRINTECH GT-LFRL-180-025-50-CC (1310)	Diameter = 1.8 mm Reflection loss ≤ 0.5 %
Photodetector	AGERE A2609C	PIN responsivity = 0.85 A/W Dark current = 10 nA @ 300K Bandwith = 40 MHz Thermistor resisteance = 10kΩ

Table 3: *The practical optical fiber components with specifications.*

6.3 Future of smart dust

Smart dust is a devise in the order of a cubic millimeter, which contains four basic components: power, computation, sensor and communication. There are a number of research institutions that are currently working on centimeter-scale distributed sensor network. Several research groups at UCLA are developing an entire radio on a single CMOS substrate and a low power wireless MEMS.

The future of smart dust lies on both optical communication and fiber-optic communication. The MEMS is one of the main technologies that can improve both communication systems. There are several obstacles in the developing a communication system for the cubic millimeter-scale distributed sensor network. Nevertheless, it stands in the way of the future commercialization of smart dust. To improve performances of the free-space optical and fiber-optic communication systems, it needs to achieve a high data rate. This can be achieved by improving MEMS techniques and a data rate of the imaging receiver.

Power consumption is also one of the major components that play a key role in design of the smart dust. While microcontroller consumes less power, battery energy densities have not improved significantly over the years. In the future, a custom circuit design of the microcontroller with the choice of electronics will allow to employ additional functionality. The additional functionality will make future smart dust to be able to perform more complex functions.

7. CONCLUSION

Smart dust is an ongoing research project whose main objective is to design a cubic millimeter-scale sensing nodes capable of bidirectional communication. The applications of miniature distributed sensor networks are numerous. Smart dust has four major components: power, computation, sensors, and communication. With these four components, a number of smart dust systems can be designed and modified depending on the applications. A communication system for smart dust is also one of the design issues depending on the applications.

The main objective of this thesis is to design a communication system that can minimize smart mote power consumption and maximize link range and the number of dust motes that can communicate simultaneously with the base station. Each dust mote is able to communicate with a central transceiver, or communicate in mote-to-mote fashion among dust motes. In this thesis, a free-space optical passive optical communication and fiber-optic communication are analyzed and compared.

Both free-space passive optical communication and fiber-optic communication systems have several advantages over other communication systems. One of the most effective advantages is that each dust mote does not need to have an onboard light source to transmit desired sensor information. This leads to the optical communication to have advantage on power consumptions. In addition, optical transceivers require relatively simple baseband analog and digital circuitry. Table 4 shows the comparison of the estimated performance of the fiber and free-space passive optical communication systems.

Since free-space passive optical communication is a wireless communication system, it will be advantageous over the wired communication systems. The number of dust motes in the particular system can be easily increased without adding the additional components in base station. In most application, the free-space passive optical communication using CCR-based transmitter is favored. Nevertheless, this communication system comprises several limitations. The communication between dust motes cannot be performed. If a given mote does have a clear line of sight to the base station, the mote would not be able to perform any communication and this would be isolated from the system. Since each CCR can only reflect a small fraction of the illuminating light beam, the rest of illuminating light is wasted. As shown in table 4, the maximum range of the free-space communication is relatively slowly increased as increasing input power. Hence, the range of the smart dust system will not easily extend beyond 1 kilometer.

Fiber-optic communication has advantages and disadvantages over a passive free-space optical communication. This communication system does not require the unbroken line-of-sight, the link directionality, and human eye safety on an interrogating laser. Each dust mote does not need to employ more than one CCR, and the communication between dust motes and a base station can be guaranteed. In addition, the peer-to-peer communication among dust motes can be performed when the application requires. As shown in table4, the maximum range of the fiber-optic communication can be easily increased as increasing input power. Hence, it has a longer range of communication link than that of a free space passive optical communication. However, fiber-optic communication has a limitation on the application. The optical fiber cables restrict the mobility of dust mote. In order to increase the number of dust motes in the particular system, base station should employ additional optical components. Hence, using fiber-optic communication, smart dust should employ the limited number of dust motes.

By using MEMS technology, the components required for these links can be improve in the future. This will yield improvements on the performance and the optimal means to manufacture of the smart dust. Depending on the application, several design options and protocols can be considered to optimize the performance of these links.

	Free-space passive optical communication			Fiber-optic communication		
# of dust motes	1-Hundreds			8		
Probability of transmission	≤ 100%			100%		
Peer-to-peer communication	No			Yes		
Wavelength	0.83 μm			1.31 μm		
Minimum detectable power	0.23 pW			9.6 nW		
Input power	1 W	5 W	10 W	0.5 mW	1 mW	2 mW
Maximum range	564.5 m	844.2 m	1003.9 m	12.6 km	16.9 km	21.2 km

Table 4: *Comparison of the estimated performance of the fiber and free-space passive optical communication.*

8. REFERENCES

[1] V. S. Hsu, J.M. Kahn, K. S. J. Pister, Wireless Communication for Smart Dust, 1998, http://robotics.eecs.berkeley.edu/~pister/SmartDust/.

[2] K. S. J. Pister, J.M. Kahn, B. E. Boser, Wireless Networks of Millimeter-Scale Sensor Nodes, 1998, http://robotics.eecs.berkeley.edu/~pister/SmartDust/.

[3] Kris Pister, Smart Dust: Autonomous sensing and communication in a cubic millimeter, http://robotics.eecs.berkeley.edu/~pister/SmartDust/.

[4] B. Warneke, B. Atwood, K. S. J. Pister, Smart Dust Mote Forerunners, Proc. IEEE Inter. Conference on MEMS, 2001.

[5] E. A. Hollar, COST Dust, M. S. Thesis in UC Berkeley, 2000.

[6] B. Warneke, M. Last, B. Liebowitz, K. S. J. Pister, Smart Dust: Communicating With a Cubic Millimeter Computer, IEEE, 2001.

[7] J.M. Kahn, R.H. Katz, K. S. J. Pister, Next Century Challenges: Mobile Networking for "Smart Dust", http://robotics.eecs.berkeley.edu/~pister/SmartDust/.

[8] P. B. Chu, N. R. Lo, E. C. Berg, K. S. J. Pister, Optical Communication Using Micro Corner Cube Relectors, IEEE workshop on MEMS, 1997.

[9] J.M. Kahn and J.R. Barry, "Wireless Infrared Communications", Proc. of the IEEE, pp. 265-298, February 1997 (Invited Paper).

[10] V. S. Hsu, J. M. Kahn, S. J. Pister, MEMS Corner Cube Retroreflector for Free-Space Optical Communications, 1991, http://robotics.eecs.berkeley.edu/~pister/.

[11] X. Zhu, V. S. Hsu, J.M. Kahn, Optical Modeling of MEMS Corner Cube Retroreflectors With Misalignment and Nonflatness, IEEE, 2002.

[12] P. B. Chu, N. R. Lo, E. C. Berg, K. S. J. Pister, Optical Communication Using Micro Corner Cube Reflectors, IEEE Inter. Workshop on MEMS, 1997.

[13] M. Born and E. Wolf, Principles of Optics, Sixth Edition, Pergamon Press, 1980.

[14] P. P. Banerjee, T. C. Poon, Principles of Applied Optics, Irwin, 1991.

[15] P. P. Banerjee, T. C. Poon, Contemporary Optical Image Processing with MATLAB, Fist Edition, Elsevier, 2001.

[16] F. L. Pedrotti, L. S. Pedrotti, Inrtoduction to Optics, Prentice-Hall, 1987.

[17] M. V. Klein, T. E. Furtak, Optics, Second Edition, John Wiley & Sons, 1986.

[18] G. P. Agrawal, Fiber-Optic Communication Systems, Second Edition, Wiley-Interscience, 1992.

[19] J.G. Proakis, Digital Communications, Third Edition, Mc-Graw Hill, 1995.

[20] J.B. Carruthers and J.M. Kahn, Angle Diversity for Nondirected Wireless Infrared Communication, subm. to IEEE Trans. on Commun., July 1997.

[21] A. Ghatak, K. Thyagarajan, Inrtoduction to Fiber Optics, Second Edition, Cambridge University Press, 1997.

[22] R. Ramaswami, K. N. Sivarajan, Optical Networks: A Practical Perspective, Morgan Kaufmann, 1998.

[23] J. H. Frans, V. K. Jain, Optical Communications: Components and Systems, CRC Press, 2000.

[24] G. Keiser, Optical Fiber Communications, Second Edition, McGraw-Hill, 1993.

[25] G. Feld, Deploying Optical Networking Components, McGraw-Hill, 2001.

[26] N. Kashima, Passive Optical Components for Optical Filter Transmission, Artech House, 1995.

[27] D. J. H. Maclean, Optical Line Systems, John Wiley & Sons, 1996.

Vita

Yunbin Song was born in Seoul, Korea on May 20, 1974. He received B.S. degree in Electronic Engineering from Virginia Polytechnic Institute and State University (Virginia Tech) in 1999. He then joined the Electrical and Computer Engineering Department at Virginia Tech as a graduate student. He joined the Fiber and Electro-Optics Research Center (FEORC) in 2001. His research interests include optical sensors, optical communication and fiber optics.